

**EXPERIMENTAL STUDY ON THE
EFFECT OF GEOTHERMAL
RESERVOIR CONDITIONS ON
THE CRYSTALLINITY AND
MINERAL COMPOSITIONS OF
KAOLINITE AND
MONTMORILLONITE SAMPLES.**

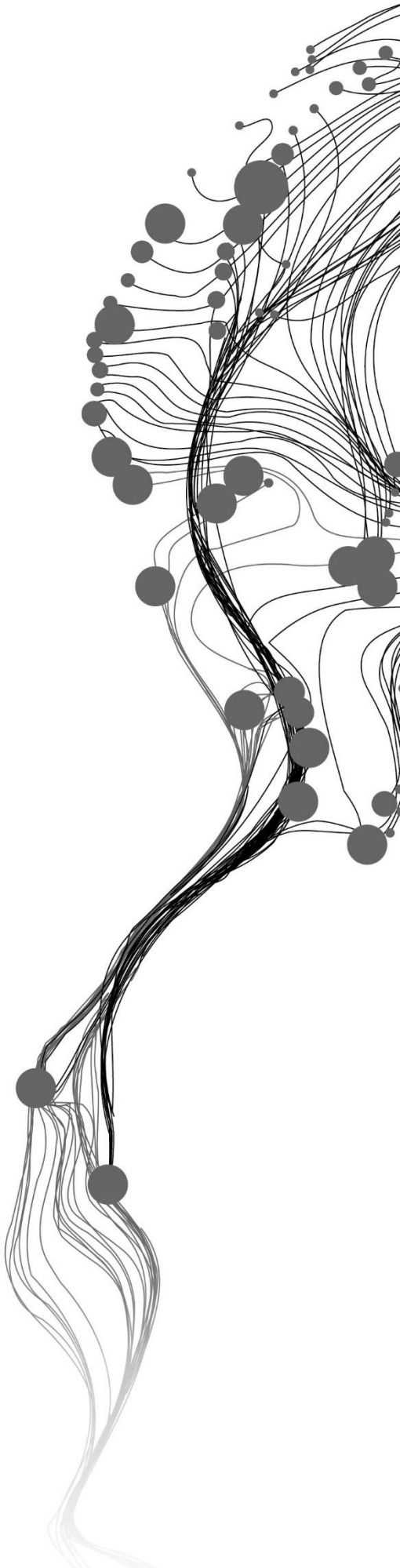
BII CHERUIYOT VINCENT

February, 2018

SUPERVISORS:

dr. C. Lievens

dr. F.J.A. Van Ruitenbeek



EXPERIMENTAL STUDY ON THE EFFECT OF GEOTHERMAL RESERVOIR CONDITIONS ON THE CRYSTALLINITY AND MINERAL COMPOSITIONS OF KAOLINITE AND MONTMORILLONITE SAMPLES.

BII CHERUIYOT VINCENT

Enschede, The Netherlands, February, 2018

Thesis submitted to the Faculty of Geo-Information Science and Earth Observation of the University of Twente in partial fulfilment of the requirements for the degree of Master of Science in Geo-information Science and Earth Observation.

Specialization: Applied Earth Sciences

SUPERVISORS:

dr. C. Lievens

dr. F.J.A. Van Ruitenbeek

THESIS ASSESSMENT BOARD:

prof. dr. M. van der Meijde (Mark) (Chair)

dr. M.W.N. (Mike) Buxton (External Examiner, TU Delft)

DISCLAIMER

This document describes work undertaken as part of a programme of study at the Faculty of Geo-Information Science and Earth Observation of the University of Twente. All views and opinions expressed therein remain the sole responsibility of the author, and do not necessarily represent those of the Faculty.

ABSTRACT

Geothermal energy potential has been widely explored in many countries and with a possibility of expansion of the existing energy production in these regions. This is so because it is considered as clean energy and thus in a bid to mitigate the effect of climate change by replacing fossil fuels. It is widely accepted as a form of sustainable energy as it helps meet decarbonization strategies and clean air. Exploration has led to discovery and exploitation of many geothermal reservoirs however some or probably quite many reservoirs do not meet expectations and show an unexpected drop in productivity over time. One of the main problem is scaling on the surface pipes. The migration of fines i.e. major and minor trace elements usually found as dissolved constituents in geothermal waters can be used as a proxy for the dissolution of minerals down in the reservoir. Scaling effect due to precipitation of minerals is another proxy for the breakdown of minerals deep down in the reservoir. However, the simulation of the scaling effect was beyond the scope of this study. This research used kaolinite with some traces of halloysite and pure montmorillonite powders to simulate clay minerals found in a geothermal reservoir caprock environment. This study also used ultrapure water of pH 7 and 1M NaCl pH 9 and 1M KOH pH 14 to simulate changes in salinity in the reservoir over time. Experimental results show that, kaolinite under the simulated conditions transforms to halloysite in presence of 1M KOH while montmorillonite changes phase to illite under the same conditions. Therefore, the study puts forward that, in an epithermal environment of high pH, kaolinite decreases in crystallinity while montmorillonite increases in crystallinity as evidenced by the phase changes. Further correlation of geochemical data like the ones from this study with geophysical data from geothermal caprock can improve the evaluation reservoir stability and life expectancy.

ACKNOWLEDGEMENTS

This thesis would not have been complete without the help of some people and an organization. First, I would like to send my gratitude to NUFFIC Netherlands Fellowship Programme for offering me the opportunity to pursue this course in The Netherlands. Secondly, my sincere appreciation goes to my supervisors dr. Caroline and dr. Frank for dire investment of their time and effort in me. The discussions and the support in the laboratory work was helpful and I learnt a lot of practices that are applicable in setting up a wonderful career ahead. Thank you again Caroline and Frank.

I would also like to acknowledge Benno and Ewout on behalf of the high-pressure lab crew that extended a helping hand despite their tight schedules to help me in setting up and correcting a few hitches in the laboratory equipment.

To the friends that I made here, especially the Kenyan community, many thanks for making my stay here warm and a home away from home. The motivational chapatis will be missed.

Finally, I would like to pass my sincere appreciation to my family for being there for me in all the moments and making the thesis progress well.

.

TABLE OF CONTENTS

1.	INTRODUCTION.....	1
1.1.	Research Background	1
1.2.	Problem definition	4
1.3.	Research objectives	4
1.4.	Research questions	5
1.5.	Hypothesis	5
1.6.	Thesis structure.....	5
2.	SAMPLES AND EXPERIMENTAL SETUP	6
2.1.	Samples and reagents	6
2.2.	Equipment	6
2.3.	Experimental conditions	6
3.	BACKGROUND INFORMATION.....	9
4.	METHODOLOGY.....	13
4.1.	Sample Acquisition.....	13
4.2.	Sample characterization.....	14
4.3.	Experimenting phase	14
4.4.	Sample extraction	15
4.5.	Oven drying.....	16
4.6.	Measurement phase.....	16
5.	RESULTS AND DISCUSSION.....	20
5.1.	XRD Result	20
5.2.	ASD Result	25
5.3.	ICP OES Result.....	31
6.	CONCLUSION AND RECOMMENDATION	34
7.	APPENDICES	v

LIST OF FIGURES

Figure 1. Diagram showing a schematic representation of the set up used to conduct the experiments in this study. The set up shows a mechanical stirrer which was not used in this study. The stirrer can be replaced with a shaking autoclave to reduce the chances of mechanical breakdown of the samples in the process of stirring. The fluidized bed was used create the heating environment during experimenting while the cooling bath was used to create the cooling environment after the experiment. (source: SPT high-pressure lab).....	7
Figure 2. Diagram showing a schematic representation of the set up used to separate the liquid from the solution after the end of the experiments in this study. The tripod stand was used to hold the autoclave firmly and at an angle allowing for a higher liquid volume as the solid would be settled at the bottom.	8
Figure 3. Conceptual diagram showing the various processes that take place in a geothermal reservoir environment from the clay caprock to the surface of the wellhead.	9
Figure 4. Diagram showing the parameters used by the XRD to characterize an unknown sample. Source; Crystal structure analysis/X-Ray Diffraction.	10
Figure 5. Diagram showing an example of an XRD pattern with basal reflections of Kaolinite, Quartz, and Illite. <i>Source; (Klosek-Wawrzyn, Malolepszy, & Murzyn, 2013)</i>	11
Figure 6. Flow diagram showing a simplified version of the methodology adopted by this research.....	13
Figure 7. Flow diagram showing the steps taken in the experimental phase of this research. A detailed flowchart together with a standard operating procedure that this study used is given in the appendix section. The solute refers to the solid samples, and the solvent refers to reagents that were used by for experiment.	15
Figure 8. Sketches showing the global areas and the reduced areas used in the calculation of crystallinity values of Kaolinite and Montmorillonite. (as provided by the XRD manual)	17
Figure 9. Diagram showing the general step used in the fusion process. This is the stage where the solid samples were digested to determine for their mineralogical composition.	18
Figure 10. Background subtracted XRD patterns of Kaolinite showing various peaks positions and intensities. The patterns were stacked in the order of +2 for Kaolinite reacted with ultrapure water(Kao.W.R.XRD) and +4 for Kaolinite reacted with 1M sodium chloride(Kao.N.R.XRD) and +6 for Kaolinite reacted with 1M potassium hydroxide(Kao.K.R.XRD) to enhance visibility of each individual pattern. The intensity scale range was set between 1 and 10 for small peak visibility. H are the peaks caused by Halloysite while K are the peaks caused by Kaolinite. Cps stands for counts per second. The question marks refer to a peak that was not identified.....	22
Figure 11. Original+background XRD patterns of Kaolinite showing the changes in the background hump in relation to the various environments exposed to. The patterns show original sample(Kao.OD.XRD), Kaolinite reacted with ultrapure water(Kao.W.R.XRD), Kaolinite reacted with 1M sodium chloride(Kao.N.R.XRD) and Kaolinite reacted with 1M potassium hydroxide(Kao.K.R.XRD) ..	22
Figure 12. Background subtracted XRD patterns of Montmorillonite residues from reaction with ultrapure water(Mont.W.R.XRD), 1M sodium chloride (Mont.N.R.XRD), and 1M potassium hydroxide(Mont.K.R.XRD). The patterns were stacked in the order of +2 for Montmorillonite reacted with ultrapure water and +4 for Montmorillonite reacted with 1M sodium chloride and +5 for Montmorillonite reacted with 1M potassium hydroxide to enhance visibility of each individual pattern. The intensity scale was set to values between -2 and 10 to show the various peaks intensities. M denotes basal reflections caused by Montmorillonite, Q denotes basal reflections caused by Quartz and I denotes reflections caused by Illite. Cps stands for counts per second.....	23

Figure 13. Original + background XRD patterns of Montmorillonite showing the changes in the background hump in the different stages of the experiment where Mont.OD.XRD refers to the original sample, Mont.W.R.XRD refers to the residue from reaction with ultrapure water, Mont.N.R.XRD refers to residue from reaction with 1M sodium chloride and Mont.K.R.XRD refers to residue from reaction with 1M potassium hydroxide. 25

Figure 14. Diagram showing the Stacked Kaolinite ASD spectra from this study where the colors; blue represents Kao.OD.ASD, green represents Kao.W.R.ASD, red represents Kao.N.R.ASD and black-Kao.K.R.ASD. The reflectance values were offset for clarity..... 26

Figure 15. diagram showing Stacked ASD spectra from the USGS spectral library showing Dickite(green), Kaolinite(red) and Halloysite(black). The reflectance values are offset for clarity, while the x axis values are the wavelength in micrometres. 27

Figure 16. Zoomed out spectra of Stacked Kaolinite ASD spectral range (2100-2250) nm of the values used to calculate crystallinity where; blue is Kao.OD.ASD, green is Kao.W.R.ASD, red is Kao.N.R.ASD and black are Kao.K.R.ASD. The values written down are the points as to which the reflectance values were used to calculate crystallinity in the equation the reflectance values are offset for clarity. 28

Figure 17. Showing stacked ASD spectra of Montmorillonite from this study showing the absorption feature positions where; blue is Mont.OD.ASD, green is Mont.W.R.ASD, red is Mont.N.R.ASD and black is Mont.K.R.ASD. The reflectance values were offset for clarity..... 29

Figure 18. Diagram showing Stacked ASD spectra of Montmorillonite from the USGS spectral library where; green is Montmorillonite, red is Illite and black is Muscovite. The reflectance values were offset for clarity..... 29

Figure 19. Spectra plot showing a continuum removed spectra of Montmorillonite in IDL DISPEC used to calculate the asymmetry of the 1400nm absorption feature used to calculate the crystallinity index of Montmorillonite. The values of the reflection extracted from the spectra are listed in appendix 2. 30

Figure 20. Zoomed spectra plot showing red -Montmorillonite reacted with 1M Sodium chloride(Mont.N.R.ASD), blue -original Montmorillonite(Mont.OD.ASD), green -Montmorillonite reacted with Ultrapure water(Mont.W.R.ASD), and black -Montmorillonite reacted with 1M potassium hydroxide(Mont.K.R.ASD). The positions stated are the ones as to which the reflectance values in the 1900nm and the 2200nm absorption feature were used to calculate the crystallinity of Montmorillonite. The values extracted are given as a table in Appendix 2..... 31

LIST OF TABLES

Table 1: Existing geothermal resources conditions sourced from literature	3
Table 2: Showing the input parameters, duration, and values of pressure temperature and pH used in this study. Kao is the unique identifier used by this study for Kaolinite while Mont is for Montmorillonite. The reagents W stands for ultrapure water, N for sodium chloride and K for potassium hydroxide.....	6
Table 3. Showing the d values and scan angles of the basal reflections attributed to Kaolinite clay mineral from this study compared to the reference datasets from the ICDD database. The angle is the scan angle in degrees and the d value is the 2-theta position in Angstrom.....	21
Table 4. Showing the d values and scan angles of the basal reflections attributed to Halloysite clay mineral from this study compared to the reference datasets from the ICDD database. The angle is the scan angle in degrees and the d value is the 2-theta position in Angstrom.....	21
Table 5. Showing the crystallinity values of each reaction from the experiment conducted with Kaolinite mineral where %C is the percentage change in crystalline content and %A is the percentage in amorphous content. The Kao.OD.XRD is the original oven dried material, Kao.W.R.XRD is Kaolinite reacted with Ultrapure water, Kao.N.R.XRD is Kaolinite reacted with 1M sodium chloride and Kao.K.R.XRD is Kaolinite reacted with 1M potassium hydroxide.....	21
Table 6. Showing the d values and scan angles of the basal reflections attributed to Montmorillonite clay mineral from this study compared to the reference datasets from the ICDD database. The angle is the scan angle in degrees and the d value is the 2-theta position in Angstrom.....	24
Table 7. Showing the d values and scan angles of the basal reflections attributed to Illite clay mineral from this study compared to the reference datasets from the ICDD database. The angle is the scan angle in degrees and the d value is the 2-theta position in Angstrom.	24
Table 8. Showing the crystallinity values of each reaction from the experiment conducted with Montmorillonite mineral where %C is the percentage change in crystalline content and %A is the percentage in amorphous content. The Mont.OD.XRD is the original oven dried material, Mont.W.R.XRD is Montmorillonite reacted with Ultrapure water, Mont.N.R.XRD is Montmorillonite reacted with 1M sodium chloride and Mont.K.R.XRD is Montmorillonite reacted with 1M potassium hydroxide.	24
Table 9. A table showing the number of ions in the formula for each element present in each Kaolinite both the original and residue calculated from the total amount in concentration. Where Mg is magnesium, Ca is calcium, Fe is iron; Al is aluminum, Si is silica. Kao.OD stands for original oven dried Kaolinite sample, Kao. W. R is the residue from the experiment with ultrapure water, Kao. N. R is the residue from the experiment with 1M sodium chloride, Kao. K. R is the residue from the experiment with 1M potassium hydroxide.	31
Table 10. Showing the number of ions for each element present in each Montmorillonite, i.e. both the original and the residue calculated form the total amount in concentration. Where Mg is magnesium, K is potassium, Ca is calcium, Fe is iron, Al is aluminum, Si is silica. Mont.OD stands for original oven dried Montmorillonite sample, Mont. W.R is the residue from the experiment of Montmorillonite with ultrapure water, Mont. N.R is the residue from the experiment of Montmorillonite with 1M sodium chloride, Mont. K.R is the residue from the experiment of Montmorillonite with 1M potassium hydroxide.	32
Table 11. Showing the extracted reflectance values for Kaolinite used to calculate the crystallinity index (KX) using the equation stated in the methodology. The three spectra were zoomed, and the values manually extracted in ENVI and recorded in the table below.....	v
Table 12. Showing extracted reflectance values for Montmorillonite used to calculate its crystallinity index using the equation stated in the methodology. The text in bold are the positions at which the reflectance	

values were extracted from. The reflectance values were manually extracted from ENVI while the asymmetry was extracted using IDL DISPEC plugin software of the same ENVI.....v

Table 13. Showing the concentration values for each element present in the original and residues of the Kaolinite sample from each experiment. Where the first values alongside each sample represent the concentration in micro gram per gram for each element.....x

Table 14. Showing the concentration values for each element present in the original and residues of the Montmorillonite samples from each experiment. Where the first values alongside each sample represent the concentration in micro gram per gram for each element.....xi

LIST OF ABBREVIATIONS

XRD –X-Ray Diffractometer

ASD –Analytical Spectral Device

ICP OES –Inductively Coupled Plasma Optical Emission Spectrum

Kao.OD –original oven dried Kaolinite sample where Kao stands for Kaolinite and OD stand for oven dried.

Kao. W. R – Kaolinite residue from an experiment with ultrapure water. Where Kao stands for Kaolinite and W stand for water and R stands for the residue

Kao. N. R –Kaolinite residue from an experiment with ultrapure water. Where Kao stands for Kaolinite and N stand for sodium chloride and R stands for the residue

Kao. K. R – Kaolinite residue from an experiment with ultrapure water. Where Kao stands for Kaolinite and K stands for potassium and R stands for the residue

Mont.OD –original oven dried Montmorillonite sample. Where Mont stands for Montmorillonite and OD stands for oven dried.

Mont. W. R –Montmorillonite residue from an experiment with ultrapure water. Where Mont stands for Montmorillonite and W stand for water and R stands for the residue

Mont. N. R –Montmorillonite residue from an experiment with ultrapure water. Where Mont stands for Montmorillonite and N stand for sodium chloride and R stands for the residue

Mont. K. R – Montmorillonite residue from an experiment with ultrapure water. Where Mont stands for Montmorillonite and K stand for potassium and R stands for the residue

Al –aluminum

Si –silica

Fe –iron.

Na –sodium

K –potassium

Ca –calcium

1. INTRODUCTION.

1.1. Research Background

Convectional geothermal systems are controlled by four main components namely, the recharge area, the heat source, the reservoir and the caprock (Corrado, Aldega, Celano, De Benedetti, & Giordano, 2014). The source of heat is usually from the earth, and some of the systems are recharged by meteoric water. In some systems, due to lack of meteoric water this system only have a hot, dry rock, and thus energy is produced by injecting cold fluids into the Hot Dry Rock (AbuAisha, Loret, & Eaton, 2016). The caprock is formed due to diagenesis and lithification. A caprock is a thick, widespread impermeable rock unit which hosts a geothermal reservoir (Corrado et al., 2014). Various processes occur at the reservoir resulting in changes in the Geothermal fluid.

Geothermal fluid composition is largely determined by various processes occurring in the reservoir including water-rock interaction, boiling, mixing, degassing (Björke, Stefánsson, & Arnórsson, 2015). Rock-water interaction with magmatic gas in the reservoir leads to dissolved constituents in the geothermal fluid. They can also result from oceanic and meteoric water (Gunnlaugsson, Ármannsson, Thorhallsson, & Steingrímsson, 2014). Geothermal reservoir interactions may involve different kinds of minerals and dissolve various metals and metalloids (Baysal & Gunduz, 2016). These interactions do lead to the presence of dissolved constituents in the geothermal fluid. The dissolved constituents have various effects on the environment due to their toxic levels. The geothermal water of western Anatolia, for example, has a high concentration of arsenic, iron, and manganese (Baba & Ármannsson, 2006; Bundschuh et al., 2013; Gunduz et al., 2012). Heavy and trace elements concentrations present in geothermal fluid also causes contamination (Baba & Ármannsson, 2006; O Gunduz, Mutlu, Elci, Simsek, & Baba, 2012). The hot and numerous dissolved constituents, if not disposed off well, can also have an effect on surface water quality (Baysal & Gunduz, 2016). Total dissolved solids in geothermal waters can also be a proxy for dissolution of minerals due to reactions down in the reservoir.

Some reservoirs are hosted by clay caprocks that have clay minerals like kaolinite in it (Patrier et al., 2013). Mostly geothermal systems are closed off by clay cap rocks (Browne, 1984). The composition of the clay cap rock, temperature variation, and chemistry of the fluid of a particular geothermal environment determine the distribution of alteration minerals in the process of geothermal energy production (Browne, 1984; Elders et al., 1984). Various authors have reported that alteration reservoir minerals include; quartz, smectite, calcite, and illite as the main hydrothermal products (Bartier et al., 2008; Hebert et al., 2010; Ledesert et al., 1993a, 1993b, 1999, 2009, 2010).

For economic extraction of geothermal energy, some systems circulate water or brine artificially through Hot Dry Rock(HDR) that are usually fractured (Haraden, 1992; Mortensen, 1978). This kind of systems are called enhanced geothermal systems. The main reason for this is to maintain reservoir pressure and avoid contamination of aquifers near the surface by these geothermal fluids (Kuè, Vernoux, Kellner, Isenbeck-Schroè, & Schulz, 1998). This circulation leads to changes in temperature and pressure resulting in shifts in chemical equilibrium (Regenspurg, Geigenmüller, Milsch, & Kühn, 2017). In the process of energy extraction and production, the brine pressure and temperature decreases which affects the chemical equilibrium of the system (Kuè et al., 1998). Such changes in equilibrium lead to drop in wellhead pressure and changes in enthalpy and non-condensable gas in steam affecting the production of energy in a particular geothermal plant (Thorhallsson, 2006).

Changes in chemical equilibrium between reservoir rocks and brine cause precipitation of various solids (Kuè et al., 1998). This is so because the cooling of saturated fluids at reservoir temperature leads to supersaturation which results in precipitation of excess concentration forming mineral deposits (Thorhallsson, 2006). Besides shifts in the chemical equilibrium, precipitation can also be caused by the complex interaction between the reservoir rock, geothermal fluid and the well casing material (Regenspurg et al., 2017). Mineral dissolution is enhanced by high temperature and pressure as a result of rock-water interactions (Baysal & Gunduz, 2016). Therefore improper design and operating conditions lead to scaling (Frick et al., 2011). Chemical stimulation also affects the caprock and fluid equilibrium resulting in either precipitation or dissolution of minerals (Ngo et al., 2016).

The precipitates formed attach themselves to pipes and other surfaces causing clogging of the systems. This results in an extra input to regain its capacity or drilling of makeup wells which in most cases are not drilled as required leading to low energy production capacity (Thorhallsson, 2006). Zhou et al. (2016) reported an average mineral dissolution of minerals causing severe issues in the reservoir and in the energy plant such as pipes clogging. The major obstacle in a geothermal system is scaling caused by metal silicates (Çelik et al., 2017). These silicates form when thermal water mix with cold groundwater which leads to a decline in the silica mineral solubility present in hydrothermal water thus leading to precipitation of silica sinter (Guo et al., 2007). Precipitation trend of minerals is also influenced by the geochemical properties of an individual geothermal system (P. Wang et al., 2016).

Corrosion, which is the undesired fluid-material interactions, is another problem that decreases the efficiency and, in some cases, can cause failure of the geothermal plant. Acidic environments result from oxidation of H_2S which leads to excessive corrosion of surface delivery pipes and wellbore pipes (Crisostomo, Villaseñor, & Calibugan, 2015). It can also occur due to induced chemical reactions which causes failure of plant components thus damaging the reservoir because of fluid reinjection (Frick et al., 2011). Low pH causes corrosion cracking in stainless steel and carbon steel corrosion (Gunnlaugsson et al., 2014). Since most of these changes are inevitable during production, a good understanding of them is vital so that one can take counter measures in time (Thorhallsson, 2006). These two problems can be attributed to the effect of operation conditions on reservoir rock- water interaction.

What goes into and comes out of the reservoir is usually measured in-situ and thus is well known however what really happens deep in the reservoir is not easily determined. However, these processes occurring down in the reservoir cannot be quantified or predicted easily due to the impossibility of access to such depths. This challenge can be attributed to high temperature and pressure in the geothermal reservoir (Kumari et al., 2017). Therefore, to understand such process and quantify, mimicking such conditions at laboratory scale is a better way to shed more light on such complex interactions at depth. An experimental set-up of high temperature, high pressure and salinity are required to simulate geothermal reservoir conditions (Regenspurg et al., 2017).

In a bid to bridge this gap laboratory analysis has been used by various authors to understand the performance of various reservoir rocks under reservoir conditions of temperature, pHs and pressure (AbuAisha et al., 2016; Kumari et al., 2017). From experimental studies, some clay minerals reaction with acid leads to splitting of particles within the octahedral sheet, i.e., leaching of aluminum, magnesium, and iron (Stuedel et al., 2009). A reaction of vermiculite and nitric acid also, for example, shows leaching of Al, Fe, and Mg from the octahedral sheet and residue of SiO_2 (Santos et al., 2015). Acid leads to release of central atoms from the octahedral sheet (Komadel, 2016). Other research showed that the Si-O bond is more stable than the Al-O bond when under pressure (Fang, Zhai, Li, Pan, & Mo, 2017).

Most fluid-rock interactions have experimented in various research with the aim of injecting carbon on different rock samples. Rosenbauer, Koksalan, & Palandri, (2005) experimented on limestone while Jedli, Jbara, Hedfi, Bouzgarrou, & Slimi, (2017) used clay, sandstone and evaporated samples. Also, Na et al.

(2016) tried analyzing the various effect of mud acid and rock interaction. The various laboratory research done, work on the mechanical dynamics of the rock samples and a further study done on clay minerals by S.A.Carroll, (2015). This shows that experimental studies on water-rock interactions to stability of the caprock to geothermal activity are still a field that needs more research.

Schmidt, Bucher, Mundhenk, & Stober, (2017) experimented on sandstone and granite using a brine. All these studies were in line with improvement and reservoir maintenance, and thus a long life of productivity. Thus, understanding such changes is vital for economical and efficient use of existing geothermal resources.

Some studies have used a combination of parameters to determine the long-term performance of geothermal reservoirs and found that fluid injection temperature affects the production temperature largely while the rate of injection pressure largely results in reservoir cooling (Aliyu & Chen, 2017). Apart from temperature and pressure, the other parameter affecting chemical evolution in a reservoir changes in pH. This is due to hydrogen sulfide and carbon dioxide leaving the liquid phase to the steam phase on boiling, and thus the liquid phase becomes more basic (Thorhallsson, 2006). Changes in pH affect mineral equilibria rendering them unstable and thus dissolve and migrate as dissolved solids in the geothermal fluid. On cooling of the geothermal fluid, the dissolved constituent precipitates. This scaling effect is prominent in the injection well mostly.

Some reservoirs are acidic due to degassing of magma gases hydrogen sulfide and carbon dioxide (Brehme, Moeck, Kamah, Zimmermann, & Sauter, 2014). Apart from hydrogen sulfide and carbon dioxide, hydrochloric acid and sulfur oxide are other volatile gases emanating from magma causing acidity in the reservoir. These gases interact with the geothermal fluid and are modified as it travels up the production well. Due to long periods of interaction with the reservoir rocks this acidic solution change in pH and become either basic or neutral (Izquierdo, Arellano, Aragón, Portugal, & Martínez, 2000).

As a guide to existing reservoir condition, this study did a literature survey of the existing geothermal resources and took an average temperature of 245 °C and pressure of 220 bars which formed the conditions for our reservoir. The various geothermal resources picked from literature shown in Table 1.

Table 1: Existing geothermal resources conditions sourced from literature

Geothermal plant	Temperature (°C)	Pressure (bar)	pH	Ions(mg/l)	Source
Lahendong	200-274	121-139	4.7-7.0	Cl 12-452, SO_4 74-114, H_{CO3} 6-68.	(Brehme et al., 2016)
	232-341	89-159	1.8-3.2	Cl (991-1559), SO_4 (523-1609)	
Wayang Windu	250-290	35-85	neutral	Cl (6000-13000)	(Bogie, Kusumah, & Wisnandary, 2008)
Iceland	180-440	75-125	5.9-6.8	(varied for each plant)	(Ármansson, 2016)
Upper Rhine Graben)	220-260	(not given)	5.02-6.67	Ca 0.345-11.7 Mg 25.2-1930 Cl 2.39-120.5	(Pauwels, Fouillac, & Fouillac, 1993)

				SO_4 76-1586	
Yangbajing	170-260	(not given)	(not given)	Cl 350-650	(S. Wang, Chuan Lu, Dawa Nan, Xiancai Hu, & Jingli Shao, 2017)
Wairakei New Zealand	~250	~12	Neutral chloride	Cl 2156 Na 1200 Ca 17.5 SO_4 25	(Hodder, 2010)
Neustadt-Glewe, (NG) Germany	98	234	5.15	Cl 131000 (Na, Ca, Mg) 83000	(Kuè et al., 1998)
U.S geothermal	150-225	(not stated)	6.4	Cl 166 Mg 0.050 SO_4 108	(C. E. Clark, Harto, Sullivan, & Wang, 2010)

Low temperatures (<150°C) were not considered for this study. Low-temperature fluids (<150°C) have a high pH of (8-10) while high-temperature fluids (>150°C) have near neutral pH of (6-8) with extremes lows of 2 and highs of 12 (Gunnlaugsson et al., 2014).

1.2. Problem definition

The clay caprock is usually the host rock of a geothermal reservoir and therefore due to the extraction of heat the delivery pipes from the wellhead to the plant clog due to precipitation of minerals. This serves as a proxy to show that something deep down in the reservoir is dissolving and being transported up the plant to the delivery pipe. The changes in temperature, pressure, and pH, deep down in the reservoir lead to the breakdown of the minerals due to changes or shifts in equilibrium. Geothermal plants are often developed, and some do not produce to the expected capacity and some even cease to operate due to failure and thus to understand the problems arising from the exploitation of the resource can aid in improved reservoir maintenance and management for sustainable development. Due to limitation by the fact that a geothermal reservoir is beneath the earth approximately over 1 kilometer and above, periodic visits to such zones is not possible. Therefore to investigate such a system, a mimic of the real system in the laboratory can serve as a tool to understand what happens or the processes that occur in such zones. Thus, therefore, this study aims to mimic a geothermal reservoir condition in the laboratory and further determine how clay minerals often found in the clay cap rock react given the various environments, i.e., a change in alkalinity or acidity of the system. Clay minerals found in the caprock are varied and differ from reservoir to reservoir. This study used kaolinite and montmorillonite to represent the clay minerals that are found in the clay cap rock.

1.3. Research objectives

Main objective

- to simulate the effect of geothermal reservoir pressure, temperature and pH (geothermal reservoir conditions) on kaolinite and montmorillonite clay minerals.

Sub-objectives.

- To determine the effect of pH on crystallinity and mineral composition of kaolinite clay samples

- To determine the effect of pH on crystallinity and mineral composition of montmorillonite clay samples
- To what degree is the simulated condition like the geothermal reservoir condition in the real world.
- To generate reaction equations that define the changes in mineralogical compositions that occurred in the autoclave.
- To combine XRD and ICP OES analytical techniques with SWIR spectroscopy in mineral characterization.

1.4. Research questions

- What is the effect of pH on the crystallinity and mineral composition of kaolinite clay samples?
- What is the effect of pH on crystallinity and mineral composition of montmorillonite clay samples?
- What are the disparities and similarities of the laboratory set up in comparison to the real geothermal system?
- Does SWIR supplement XRD and ICP OES analytical techniques in determination of phases changes as a result of experimenting.

1.5. Hypothesis

- ❖ The exposure of kaolinite to ultrapure water and 1M sodium chloride will lead to low changes in crystallinity and mineral composition, unlike 1M potassium hydroxide solution.
- ❖ Potassium hydroxide will dissolve SiO_2 tetrahedral sheet leaving corundum in kaolinite and Al, Fe, and Mg in montmorillonite.
- ❖ The use of extreme pH environments will speed up the change or alteration of the pure clay minerals.

1.6. Thesis structure

This write up consists of six chapters namely; the **introduction** which states the problem associated with geothermal plants and processes involved, the **samples and experimental set up** chapter which details the instruments and samples used by this study, the **background information** chapter which sheds more light on the concepts used in characterization and the definition of the clay minerals used in this study, the **methodology** chapter which talks about the procedures and steps used by this study, the **results and discussion** chapter talking about output and discussion and the last chapter on **conclusion and recommendation**.

2. SAMPLES AND EXPERIMENTAL SETUP.

2.1. Samples and reagents

This research used two clay minerals namely kaolinite and montmorillonite in the simulation. To simulate the changes in pH this research used three reagents which include; ultrapure water, 1M potassium hydroxide, and 1M sodium chloride. The montmorillonite was pure while the kaolinite had some traces of halloysite in it. The way the concentrations of 1M sodium chloride and 1M potassium hydroxide were made is given in the appendix.

2.2. Equipment

The main components that the research used in experimenting include; an Autoclave-a 45ml high pressure (600 bars max) and high temperature (600°C) reactor which was used to provide an environment for the simulation process. A syringe with a 0.45µm Millipore filter was used to suck out the liquid fraction from the solution before scooping out the solid out of the reactor using a scoop. Both the liquid fraction and solid fraction were stored in 40ml clear bottles awaiting analysis. A schematic diagram of the experimental set up is shown in Figure 1. Table 2 provided below details the input parameters that were used in the experiment

2.3. Experimental conditions

The various input parameters used to conduct the experiment are shown in Table 2. The starting pressure was used to reach the desired pressures of approximately 220 bars.

Table 2: Showing the input parameters, duration, and values of pressure temperature and pH used in this study. Kao is the unique identifier used by this study for kaolinite while Mont is for montmorillonite. The reagents W stands for ultrapure water, N for sodium chloride and K for potassium hydroxide.

Mineral	Reagent	pH	Starting pressure(bars)	Pressure (bar)	Temperature (°C)	Duration (days)
Kao	W	7	96	221	248	6
Kao	N	9	96	227	245	6
Kao	K	14	96	218	248	6
Mont	W	7	96	233	245	6
Mont	N	9	96	236	247	6
Mont	K	14	96	248	247	6

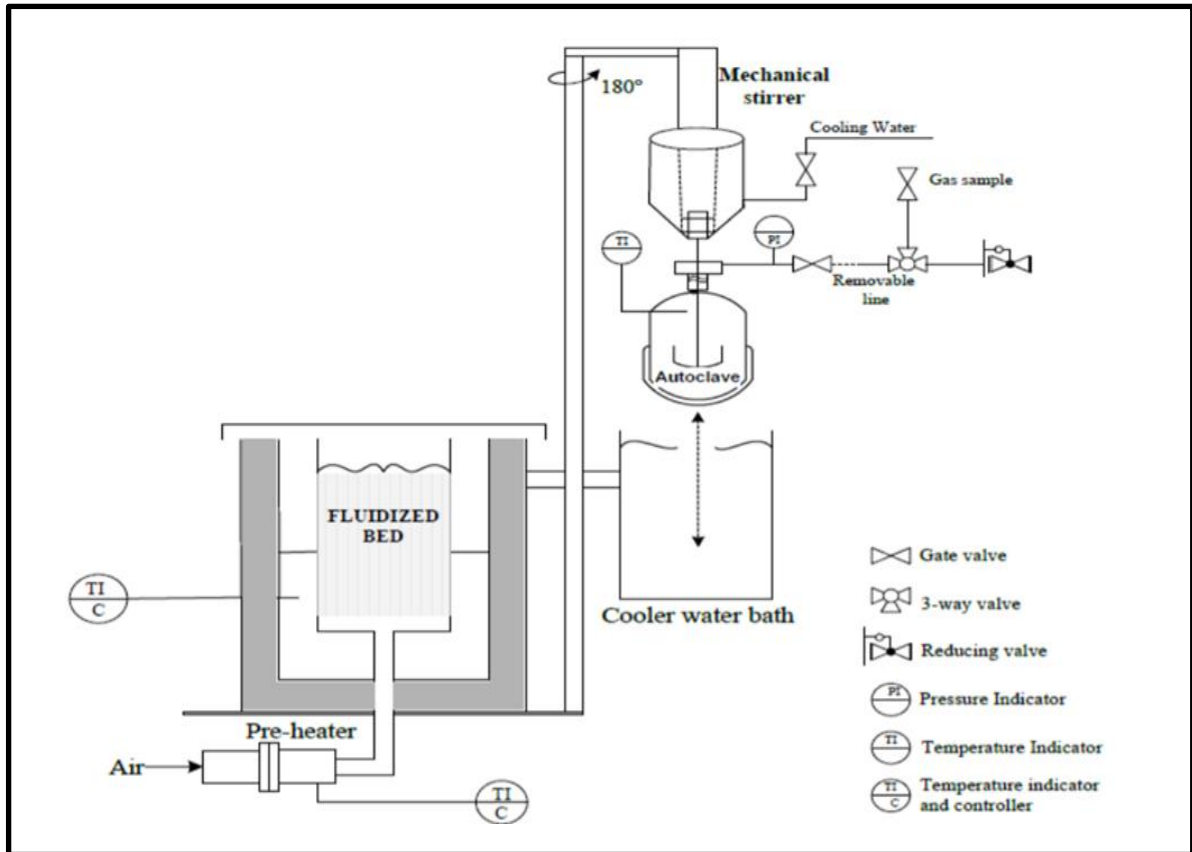


Figure 1. Diagram showing a schematic representation of the set up used to conduct the experiments in this study. The set up shows a mechanical stirrer which was not used in this study. The stirrer can be replaced with a shaking autoclave to reduce the chances of mechanical breakdown of the samples in the process of stirring. The fluidized bed was used create the heating environment during experimenting while the cooling bath was used to create the cooling environment after the experiment. (source: SPT high-pressure lab)

A detailed explanation of the operation of the above set up is given in the methodology and attached in the appendix is the standard operating procedure for operating the same setup. To separate the liquid and solid that was present in the solution the set up shown in Figure 2 was used. To reduce the contamination, a long syringe was used to suck out the liquid from the autoclave directly, and the solid scooped out of the autoclave using a long scoop spoon. The remaining solids in the autoclave were washed out using the 10ml of ultrapure water.

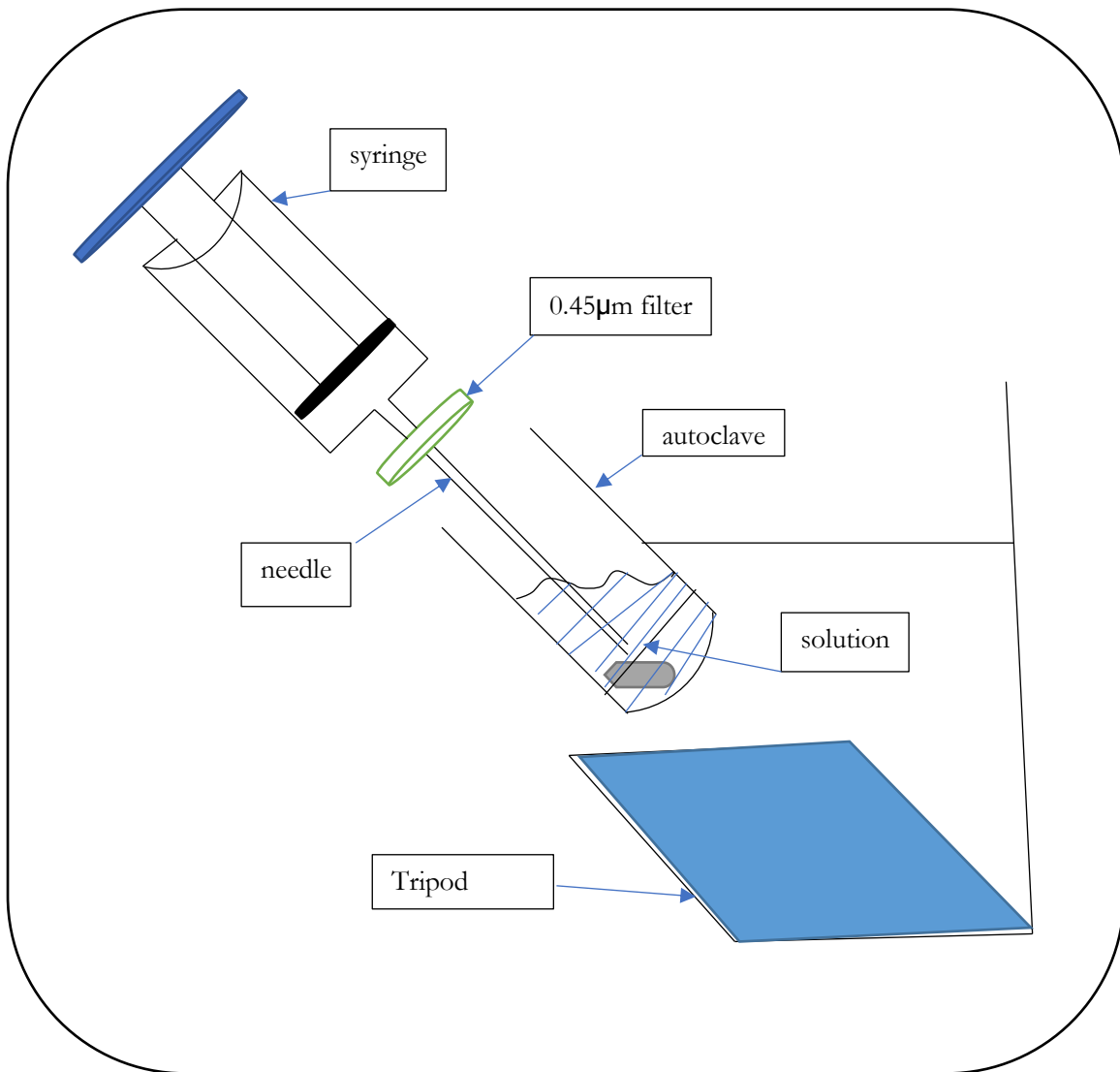


Figure 2. Diagram showing a schematic representation of the set up used to separate the liquid from the solution after the end of the experiments in this study. The tripod stand was used to hold the autoclave firmly and at an angle allowing for a higher liquid volume as the solid would be settled at the bottom.

3. BACKGROUND INFORMATION.

Due to heating, clay minerals found in sandstones and shales undergo very low-grade metamorphism and diagenetic reactions (Corrado et al., 2014). After diagenesis, the sediments integrate to form a rock through a process called lithification. An example of the rocks formed is a clay caprock which hosts a geothermal reservoir. The composition of the clay cap rock, temperature variation, and chemistry of the fluid of a particular geothermal environment determine the distribution of alteration minerals (Browne, 1984; Elders et al., 1984). Various authors have reported that alteration reservoir minerals include; quartz, smectite, calcite, and illite as the main hydrothermal products (Bartier et al., 2008; Hebert et al., 2010; Ledesert et al., 1993a, 1993b, 1999, 2009, 2010). Some Geothermal and Epithermal deposits have reported the presence of kaolinite, and Illite Smectite mixed clay minerals thus indicating the alteration assemblages (Canet et al., 2015).

In Geothermal systems, due to pressure, temperature and salinity, different kinds of minerals form. Due to loss of magmatic gases like CO_2 and H_2S , there is presence of an increase in salinity and acidity in the system leading for formation of some minerals like kaolinite while montmorillonite forms in neutral pH environments (Hedenquist, Arribas, & Gonzalez-Urien, 2000). Some clay caprocks are closed off via montmorillonite and kaolinite clay minerals. A schematic diagram is shown in Figure 3 illustrating the concept and model of a typical geothermal environment below the earth surface to variable depth of approximately 2.5km. The schematic diagram seeks to explain the processes that are typical in a geothermal reservoir environment.

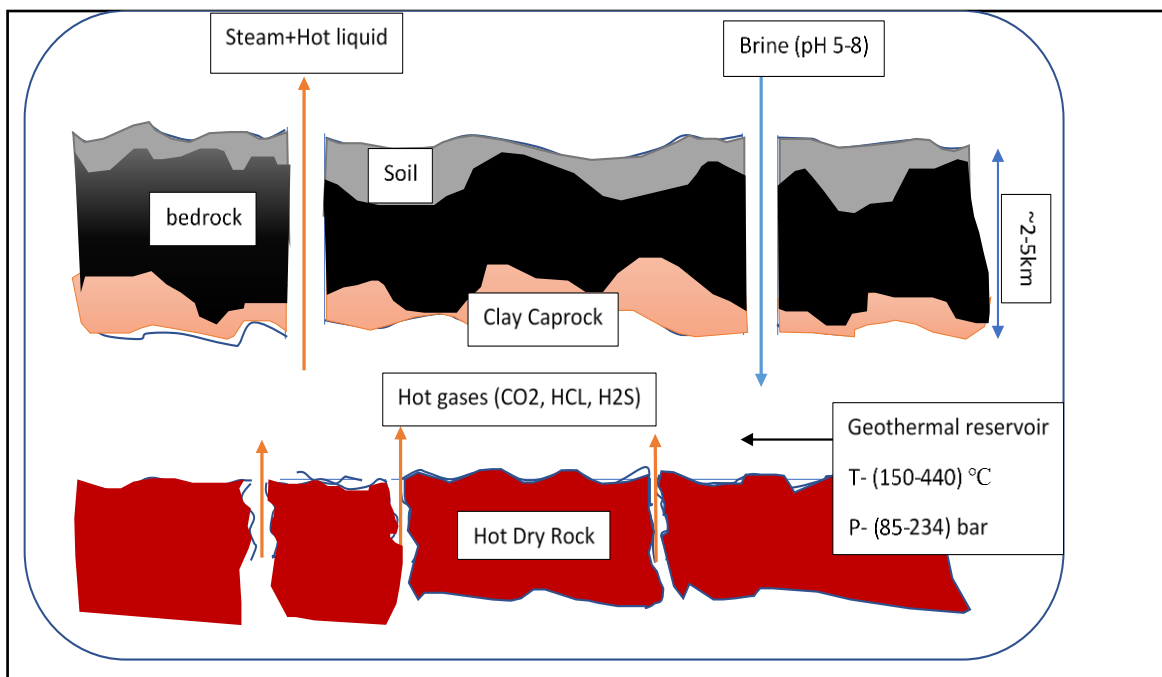


Figure 3. Conceptual diagram showing the various processes that take place in a geothermal reservoir environment from the clay caprock to the surface of the wellhead.

Kaolinite clay mineral is a clay mineral that is formed by chemical weathering of aluminum silicate minerals like feldspar. It is a layered silicate mineral consisting of one aluminum octahedral sheet and one tetrahedral silica sheet hence the name 1:1. The molecular formula of kaolinite is $Si_2Al_2O_5(OH)_4$. This is the idealized formulae which shows that it has 9 oxygen atoms. Montmorillonite is a clay mineral from the smectite group. It has two silica tetrahedral sheets and one aluminium octahedral sheet in between the two

tetrahedral sheets hence the name 2:1. The molecular formula of montmorillonite is

$(Na\ Ca)_{0.33}(Al\ Mg\ Fe)_2Si_4O_{10}(OH)_2 \cdot nH_2O$. The idealized montmorillonite chemical formula has 13 oxygen atoms as shown above.

Characterization of these clay minerals has proved a vital tool in understanding the nature and composition of such minerals that are not visible to the human eye. Equipment used in the characterization include ASD, XRD and ICP OES. The XRD uses the interplanar distance between crystals to identify the particular unknown sample. This is called the d spacing measured in Angstroms(Å). Figure 4 shows all the parameters used by the XRD to characterize a sample. The principle behind this is that waves hitting the crystal lattice of a mineral get scattered at angles. Crystals produce intense reflected radiation at specific wavelengths and incident angles thus making mineral characterization by XRD possible.

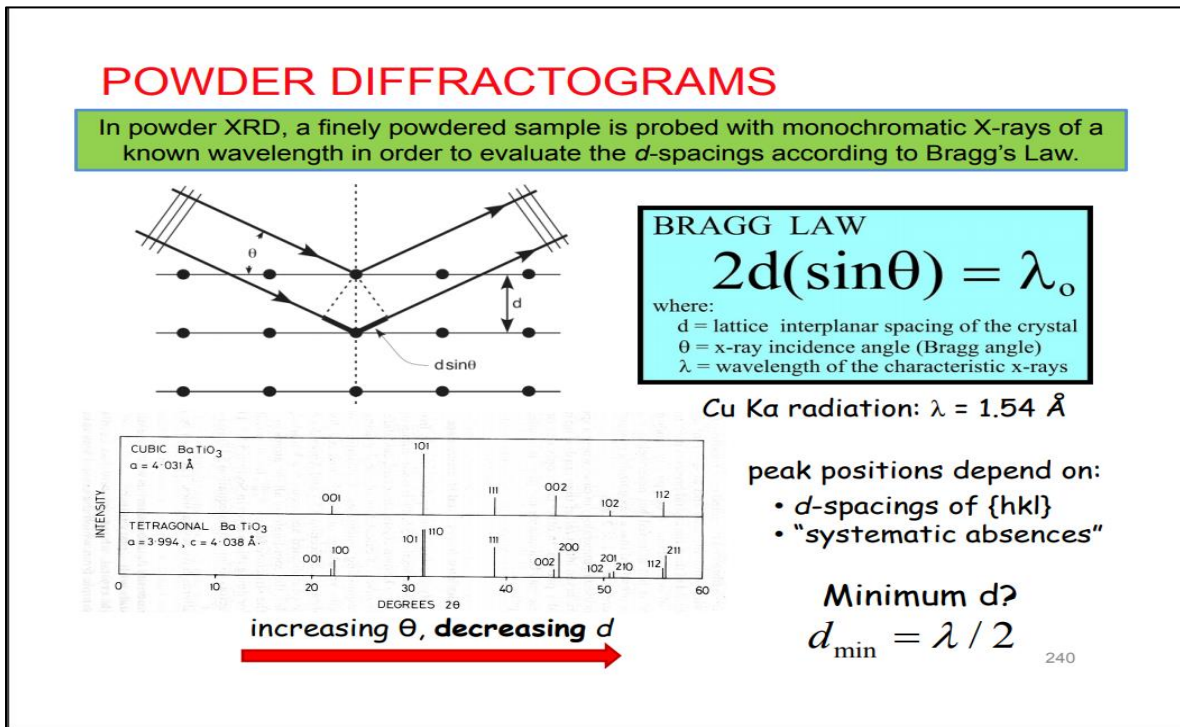


Figure 4. Diagram showing the parameters used by the XRD to characterize an unknown sample. Source; Crystal structure analysis/X-Ray Diffraction.

Different minerals have different d spacings as shown in Figure 5. Kaolinite, for example, has distinct peaks at 7.18Å and 3.57Å (Canet et al., 2015).

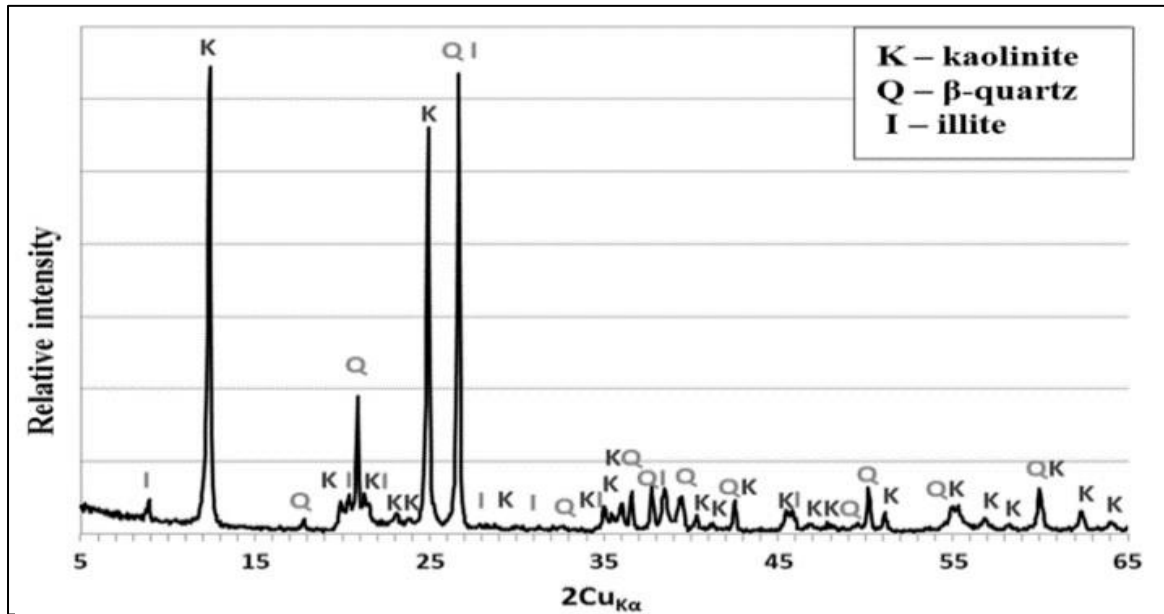


Figure 5. Diagram showing an example of an XRD pattern with basal reflections of kaolinite, quartz, and illite. *Source: (Klosek-Wawrzyn, Malolepszy, & Murzyn, 2013)*

Using the ASD, various minerals can be identified based on their absorption features. In essence, the absorption feature parameters, i.e., wavelength depth relates to material relative abundance while wavelength position defines the type of material it is (Kopačková & Koucká, 2017). The positions of interest in the entire spectral range are the VNIR(400-1000nm) and the SWIR(2000-2400nm). The absorption features in clay minerals occur in the VNIR regions due to the transfer of charges in the transition elements while in the SWIR regions is due to stretching and bending of bonds in hydrous minerals (Rani, Ravibabu Mandla, & Singh, 2017). Kaolinite mineral has characteristic doublets in the 1400nm and 2200nm absorptions. The characteristic doublets relate to the degree of kaolinite crystallinity. These minerals have bonds, i.e., Al-OH at 2.2µm and (Fe, Mg)-OH at 2.3µm (R. N. Clark, King, Klejwa, Swayze, & Vergo, 1990).

Kaolinite minerals are defined by their characteristic absorptions related to OH stretching bonds at the 1400nm and 2200nm (Garcia, 2013). Kaolinite mineral is well structured and thus has a minimum absorption feature that is almost absent in the 1900nm. X-ray diffraction and SWIR has been used to characterize kaolinite crystallinity due to the development of OH bands position (Crowley & Vergo, 1988). The characteristic doublets of kaolinite in the Al-OH feature is used to determine the crystallinity degree (Garcia, 2013). To calculate the crystallinity of kaolinite the following equation was used

$$KX = \left(\frac{R_{2166}}{R_{2177}} \right) - \left(\left(\frac{R_{2184}}{R_{2190}} \right) - \left(\frac{R_{2166}}{R_{2177}} \right) \right) \quad \text{Equation 1. Modified after (Garcia, 2013)}$$

Montmorillonite can be characterized due to the vibrations of the water and the OH- ion(Garcia, 2013). The depth of the absorption feature at the 1400nm and 1900nm show the position and content of water as they not only have deeper but also broader features compared to other minerals in the smectite group like illite and from the kaolinite group (Kruse & Hauff, 1991; Post & Noble, 1993). The presence of ions, i.e., Fe and Mg in montmorillonite causes vibrations due to their substitutions in the region between 2350-2450nm while Al content vibrations are registered in the 2200nm feature (R. N. Clark et al., 1990; Duke, 1994). Montmorillonite has four distinct absorption features.

The most commonly used technique to determine the crystallinity of montmorillonite is the XRD which defines this crystallinity based on the interlayer spacing (Garcia, 2013). This technique is dependent on the particle size of the measured samples, and thus this study used a homogeneous sample in the analysis. To complement for the crystallinity changes, SWIR spectrometry, which measures the crystallinity degree in

the crystal lattice, using depths of absorption features due to water, OH and Al-OH bonds, can be used (Kruse & Hauff, 1991).

For montmorillonite, the degree of crystallinity can be calculated using the ratio of 2200D/1900D related to the 2200W which is used as an indicator of aluminum and water content (Duke, 1994; van Ruitenbeek, Cudahy, Hale, & van der Meer, 2005). Apart from the 2200D/1900D above, another factor used in determining the crystallinity of montmorillonite is the 1400nm feature as it is an indicator of the water content present in the mineral. The more the water in the crystal lattice, the broader the feature, the longer the wavelength thus indicating less crystalline structures (Garcia, 2013). To calculate the crystallinity index of montmorillonite the following equation is used:

$$(1 + 1400AS) * \left(\frac{2200D}{1900D}\right) \quad \text{Equation 2. After (Garcia, 2013).}$$

The 1400AS feature was extracted using the IDL DISPEC software as shown in figure 14. (IDL DISPEC is an IDL plugin in ENVI developed by ITC 's Harald van der Werff, Freek van der Meer and Steven de Jong)

4. METHODOLOGY.

To obtain its objectives, this research used a general set of steps which involved running the experiment using an autoclave at the University of Twente's High-Pressure Laboratory and conducting sample characterization and analysis at the ITC Geoscience laboratory. The duration of each experiment was 6 days. A general flow chart of the steps taken is shown in Figure 6. The general methodology involved the following steps, i.e., sample acquisition, sample characterization, experimental phase, sample extraction, oven drying of the solid samples and the measurement and analysis phase.

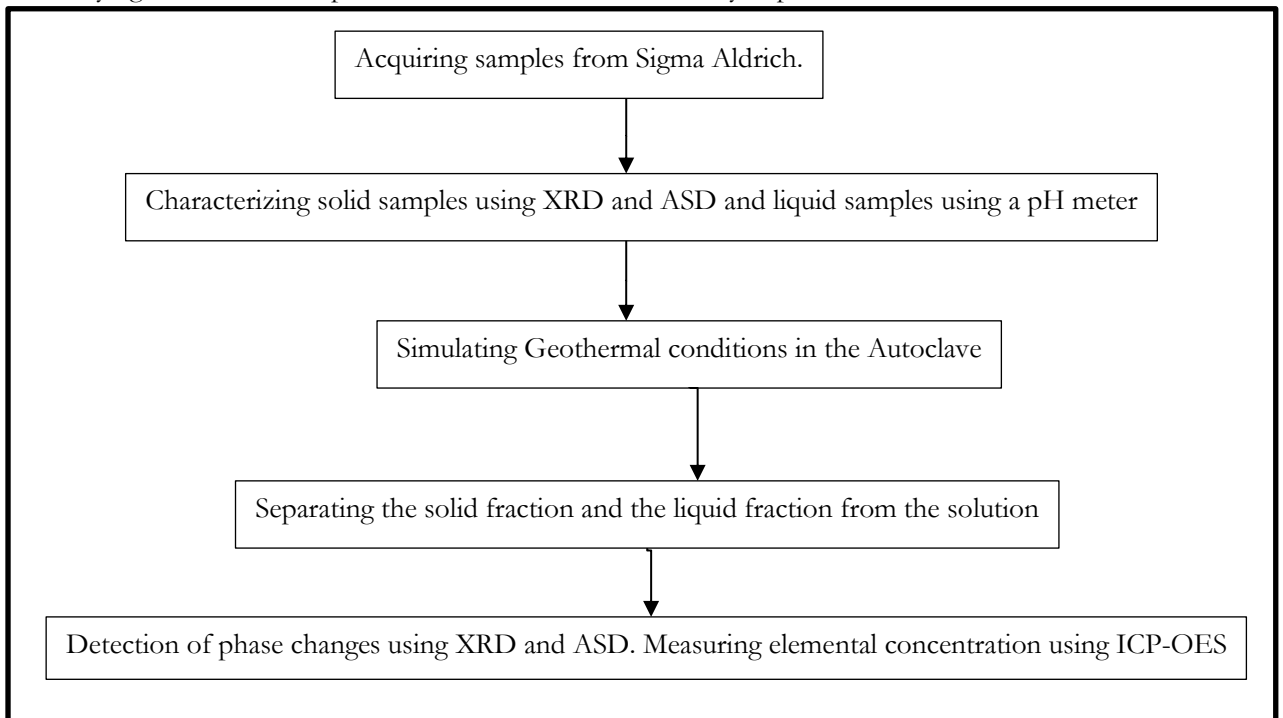


Figure 6. Flow diagram showing a simplified version of the methodology adopted by this research.

4.1. Sample Acquisition

The clay mineral samples that were used by this research were provided by the ITC Geoscience laboratory. The kaolinite clay sample was present in the laboratory and had been acquired from MERCK company. It was a bole white powder and extra pure with low bacterial content. The montmorillonite sample was bought from Sigma Aldrich Company. It had a pH of 3-4 and in powder form. These values were written in the container holding this solid as provided by the supplier. Since both samples were in powder form, they were used directly without any other particle size modification. Ultrapure water and sodium chloride crystals were provided by the ITC Geoscience laboratory. The sodium chloride crystals were extra pure with a pH of 5.0-7.5. It had been acquired from the MERCK company. Potassium hydroxide pellets that were used in this study were present in the High-pressure laboratory at the University of Twente. They had been acquired from Sigma Aldrich company. It had a pH of 14, and it was pure. The weights and ways used to prepare the molar concentrations of reagents used in this study are given in the appendix section as appendix 1.

4.2. Sample characterization

The solid clay mineral samples were tested for their purity and phases present by use of X-Ray Diffraction(XRD) and Analytical Spectra Device devices(ASD) at the ITC Geoscience Laboratory. Two XRD Petri dishes and a spatula were cleaned using a dry laboratory towel. Kaolinite clay mineral was put on the dish, and it was put in the XRD for measuring. The slit parameters and duration used were adjusted to obtain patterns from 6° to 80° (degrees 2θ), with steps of 0.012° and each step for 0.1 sec. A detector slit of 8mm was used, the divergence slit used was 0.6mm and knife was 1mm. Each scan was conducted for 30 minutes. The XRD was set to autorepeat, and thus one measurement per sample was taken. The same procedure was applied for montmorillonite clay mineral. After the XRD measurement, the Petri dishes with the analyzed samples from XRD were measured by the ASD. Two measurements were taken for each sample by the ASD. Regular calibration was done by taking a white reference measurement in between the clay mineral sample measurements to reduce effects caused by changes in heating up of the detector of the equipment. After these measurements, the clay mineral samples were disposed off to the respective bins. The Petri dishes were cleaned, and dried using a dry lab towel and stored back in the sample holder box.

After characterization of the solid samples, 30g of each clay mineral, i.e., kaolinite and montmorillonite were scooped from the original sample container and put in clean plastic bottles for transport to the High-Pressure laboratory at the University of Twente. 100g of each of the reagents, i.e., 1molar sodium chloride, and one molar potassium hydroxide, were prepared at the High-Pressure laboratory's fumehood. The pH of the reagents was measured using a Metrom 744 pH meter using a calibration line of pH4 and pH7. The reagents were put in clean glass bottles and stored in their respective cupboards.

4.3. Experimenting phase

At the High-Pressure laboratory, the autoclave was rinsed three times with tap water, three times Aqua Regia, three times distilled water. Compressed air and a dry lab towel were used to dry the autoclave. The bottom cap of the autoclave was then screwed to the main body of the autoclave. The weight of the empty autoclave was then measured. 15g of reagent (ultrapure water or sodium chloride or potassium hydroxide) was measured and added into the autoclave. 5g of solute (kaolinite or montmorillonite) was then measured and added into the autoclave. The total weight of the autoclave with both the solute and solvent was taken. The top cap of the autoclave was then screwed onto the main body and the autoclave attached to the mount inside the pressure box (box is a term used by the high-pressure laboratory to denote the room at which the experiment is conducted. It was also referred to as a bunker). A thermocouple and a pressure gauge that were directly connected to a computer outside the box were then connected to the autoclave.

Nitrogen gas was used to build pressure in the autoclave. An external pressure inlet pipe from the Nitrogen gas supply tank was then connected to the mount and the pressure valve on the mount open to allow pressure into the autoclave. The system was then flushed thrice with a pressure of 200 bars. This was to detect any leakages in the system and expel any oxygen from the autoclave. The pressure valve on the mount was closed. A spray present in the box was used to detect for the leakages. Any bubbles signified some pressure loss while no bubbles signified a tightly closed system. Any leaks from the inlet pressure pipe joint were not considered a leak because this pipe was always detached from the mount once the desired pressure for the experiment was reached. The most important parts that were checked for leakages were the thermocouple and pressure valves on the autoclave.

96 bars of pressure, which was the desired pressure was then added to the autoclave and the gas inlet pipe detached from the mount. A random check on all the moveable wires was conducted to ensure that they are all free to move without any obstacles. On satisfaction with the setup, the box was closed, and from outside the box the oven temperature was set to 260°C. For this project, the fluidization was already

heated to 300°C, and thus no further modification was done on the preheater temperature. For purposes of starting up the preheater system, a detailed standard operating procedure is added as an appendix to this document. The autoclave was then lowered to the fluidization bed and left running for 6 days. The starting pressure and temperature were recorded, and periodic checks in the system were done until the end of the experiment.

On the 6th day, the experiment was stopped. The final temperature and pressure were recorded, and the autoclave was lifted out of the fluidization bed and lowered into a cooling bath and left until the temperature in the autoclave reached room temperature, and the pressure dropped to a value close to the starting pressure of 96 bars. When these conditions were met, the box was now safe to enter. The inlet pressure line was connected, and the pressure valve opened to release the 96bars in the autoclave to an atmospheric pressure of 1 bar. The thermocouple, gas inlet pipe and the pressure valve connected to the autoclave were detached from the autoclave, and the autoclave detached from the mount as well. The top cap of the autoclave was unscrewed and the solution in the autoclave taken for extraction. The same procedure was used for all the experiments conducted by this study. A total of 6 experiments were conducted by this study. A flowchart showing the steps undertaken by this study is given in Figure 7. A detailed flowchart including the position and number of measurements done and the number of samples used is provided as an appendix to this document.

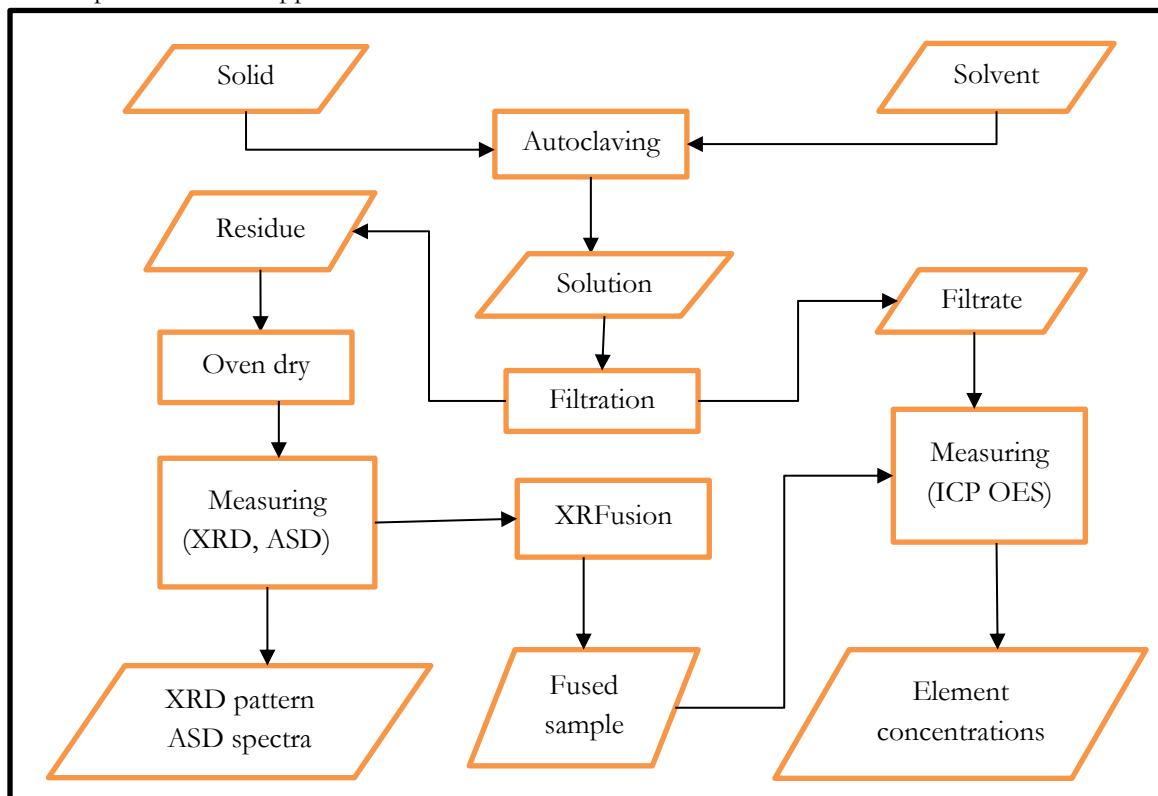


Figure 7. Flow diagram showing the steps taken in the experimental phase of this research. A detailed flowchart together with a standard operating procedure that this study used is given in the appendix section. The solute refers to the solid samples, and the solvent refers to reagents that were used by for experiment.

4.4. Sample extraction

The weight of the autoclave plus the solution was measured. Two glass bottles were cleaned ready for holding the solid and liquid extracted from the solution. The weight of the empty bottles and a 0.45µm Millipore filter were taken. The liquid was sucked out using the 0.45µm Millipore filter connected to a

syringe and long needle. The liquid extracted was put in one of the glass bottles. The solid sample was scooped out from the autoclave and put in the other glass bottle as well. The final solid attracted to the walls of the autoclave was rinsed with 10g of distilled water. The weight of the empty autoclave, number of and weight of used Millipore filters, the weight of the bottle with the filtrate, and weight of the bottle with the wet residue was taken down. The filtrate and the residue were transported to the ITC Geoscience laboratory for analysis and measurement.

4.5. Oven drying.

Before any analysis was conducted both the original samples, i.e. kaolinite and montmorillonite not put through any experiment and the residues, i.e. kaolinite and montmorillonite from the experiments were oven dried at the ITC Geoscience laboratory overnight for a period of 16hrs at 105°C. The weight of the residues after oven drying was recorded to determine the final weight of the solid. The solids were now set ready for measurement.

4.6. Measurement phase.

4.6.1. XRD analysis

The XRD machine was turned on and left to start up for one hour. The equipment used was a Bruker D2 Phaser XRD with a source of Cu K α at 30 kV and 10 mA. Meanwhile, 2 XRD sample holders, a square glass, and a spatula were cleaned using a dry lab towel. The spatula was used to scoop some dry solid onto the sample holders. The square glass was used to level the solids on the samples holders and pressed firmly to prevent preferred orientation of the samples. When the device was ready, the settings were adjusted to obtain patterns from 6° to 80° (degrees 2 θ), with steps of 0.012° and each step for 0.1 sec. A detector slit of 8mm was used, the divergence slit used was 0.6mm and knife was 1mm. The autorepeat setting of the machine was turned on. Two samples were prepared for each residue and measured for 30 minutes. This resulted in patterns that were exported as XY scans for analysis in excel. The duplicate scans were averaged by adding the intensities of each of the two scans and dividing the total value by two. A qualitative analysis was conducted to determine the changes in the overall crystallinity of the phases present in comparison to the original due to the conditions under which the minerals were exposed to. To identify the phases, present in the minerals, using the program EVA DIFFRAC suite, a threshold was set which gives all the peaks from the pattern using the search peaks option. Using these peaks, a search/match was performed by comparing the patterns from this research, and those from the ICDD database and the most potential phases present in the clay mineral sample were picked. To perform a comparison analysis and interpretation, each pattern peak was made into a DIF file and printed as pdf. This DIF file comes with all the values of each pattern from the stick number, stick position in the pattern, d value of the stick and intensity of the stick. A stick here refers to the peaks in the patterns as presented by the software. To identify and characterize the phases present in the clay mineral this study used reflections with over 50% intensity across the reference and the sample patterns.

To calculate for crystallinity, the following equations that are provided by the XRD manuals were used. Figure 8 shows the regions that were used to calculate the values for crystallinity for each mineral. Whereby each peak arising on top of the background hump i.e. reduced area is subtracted from the background hump and taken as a percentage as shown in equation 3 and 4 below.

$$\%Amorphous = \frac{Global\ area - Reduced\ area}{Global\ area} \times 100 \quad \text{Equation 3}$$

$$\%Crystallinity = 100 - \%Amorphous \quad \text{Equation 4}$$

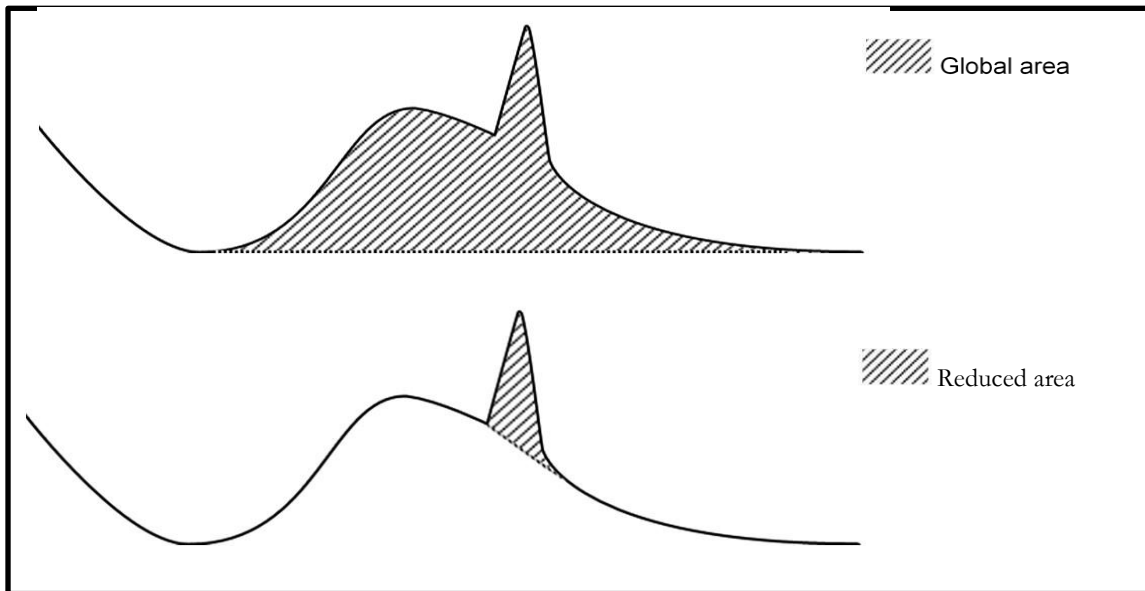


Figure 8. Sketches showing the global areas and the reduced areas used in the calculation of crystallinity values of kaolinite and montmorillonite. (as provided by the XRD manual)

4.6.2. ASD analysis

The equipment used was the ASD Spectrometers FieldSpec 3 which has a spectral range of 350-2500nm and a spectral resolution of 3nm at 700nm and 10nm at 1400-2100nm present at the ITC Geoscience laboratory. The sampling interval of the equipment was 1.4nm for the VNIR and 2nm SWIR. Immediately after the XRD measurements, the two samples in the XRD sample holders were taken for ASD measurements. The outer diameter of the contact probe was 2.75cm, and the inner diameter was 2.0cm while the diameter of the XRD sample holder was 2.5cm. Two measurements per sample were taken using the RS3 software. To preserve the quality of the measurements, a dark current and white reference measurement were taken in that order, i.e., regular re-calibration, was done in between the measurements. A splice correction was then done, and the files exported in ASCII format using the ViewSpec software. This double reflectance measurement values for each kaolinite and montmorillonite as text files were added and divided by two in excel and saved as text files. Using the spectral library builder tool from ENVI software, the text files were imported, and a spectral library was created. The equations 1 and 2 provided above were used to calculate the crystallinity changes in the kaolinite and montmorillonite clay minerals. Manual interpretation was employed in extraction of the reflectance values used in calculating the crystallinity

4.6.3. ICP OES analysis

As a complement to the ASD and XRD measurement, the Inductively Coupled Plasma Optical Emission spectrometry(ICP-OES) was used to detect trace elements in the liquid fraction, i.e., filtrate from the experiment. The equipment used in the analysis was the ICP/OES (Perkin Elmer 8300DV). To further understand the concentration of elements, present in the clay minerals, 0.1g of kaolinite in the XRD sample holder was mixed with 1g of flux and digested in 50ml 10% nitric acid in the xrfuse 2 Fusion machine. The general methodology used is shown in Figure 9.

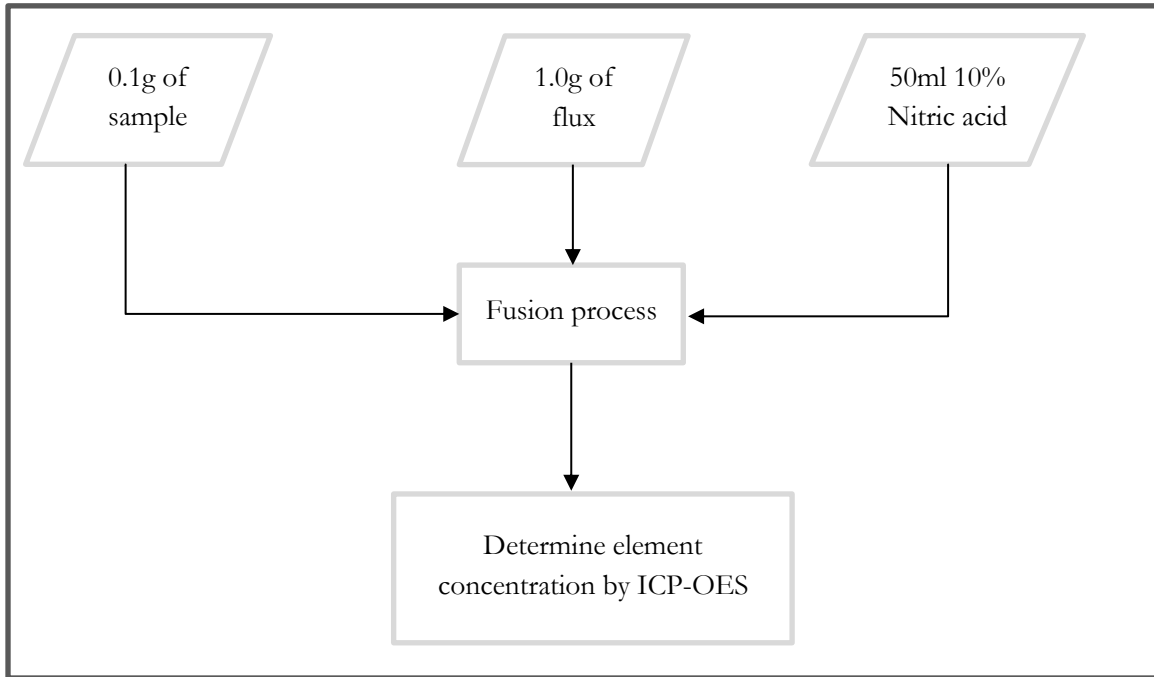


Figure 9. Diagram showing the general step used in the fusion process. This is the stage where the solid samples were digested to determine for their mineralogical composition.

The kaolinite digested was both the original sample and the residues from the experiments. The same procedure used for kaolinite was applied to montmorillonite. The elements under investigation were Aluminium (Al), Silica (Si) and Magnesium (Mg), Calcium (Ca), Sodium (Na), Iron (Fe) and Potassium (K). In some instances, there was a residue from the fusion process; this residue was then put in a watch glass and its weight taken. The weight of the residue was subtracted from the mass of the sample used before calculation of the elemental concentration was done. A solution containing only 1.0g flux and 10% nitric acid was used as a blank reagent for the fusion process. The blanks for the experiment included, ultrapure water, 1M sodium chloride, 1M potassium hydroxide and 1M hydrochloric acid. All the blanks were subtracted from the ICP measurement and before the concentration of the elements calculated. Each liquid sample set in for ICP measurement was done in duplicate. Some of the elements recorded concentration values above and below the calibration lines. The calibration lines used for this study was minimum of 0.000µg/ml and maximum of 100µg/ml. Values above the maximum calibration line were diluted 20 times to get the exact element concentration. The values below the minimum calibration line, i.e., negative values were not used in this study.

The equation used to calculate the concentration of elements in the clay minerals was

$$\text{Concentration } (C) = \frac{\mu\text{g/ml} \times 50\text{ml}}{(\text{mass of flux} + \text{mass of sample}) - \text{residue}} \quad \text{Equation 5.}$$

Where µg/ml was the ICP OES result element concentration after subtracting the blank fusion multiplied by the volume of 10% Nitric acid (50ml) used then divided by the mass of solute in grams. This was done to determine the changes in mineral composition because of changes in the conditions during the experiment.

To calculate the chemical formulae from the mineral analysis, the following steps were followed.

- The percentage weight each of the constituent oxide was calculated from the concentration values
- The percentage weight of the oxides was then divided by the molecular weight of each oxide to get the molecular proportions of the oxides

- The molecular proportions of the oxides were then multiplied by the number of oxygens in the concerned oxide to get a number that is proportional to the number of oxygen atoms present in the elements under study
- The sum of the proportional number was determined, and the total number of oxygen atoms present in the idealized formulae was calculated. The number of oxygen atoms present in the idealized formulae was then divided by the sum of the proportional number. This was done to recast the oxygen atom from each element to tally with the total number of oxygen in the idealized formulae.
- The number of cations that are associated with each oxygen atom was then calculated. These values were then used to calculate the final chemical formulae.

5. RESULTS AND DISCUSSION.

5.1. XRD Result

From characterization of the original samples, i.e., kaolinite and montmorillonite using XRD and ASD the montmorillonite mineral was found to be pure, i.e., it was the only phase present in the sample while the kaolinite was mixed with some traces of halloysite. This conclusion was reached after a qualitative analysis was made by comparing the scans from this research and those from the crystallographic database. As shown in Figure 10 the pattern has a distinct basal reflection at 8.783° $d=10.060 \text{ \AA}$. This peak reflection was caused by halloysite. Together with this peak, another distinct peak in the clay mineral was at 17.669° $d=5.018 \text{ \AA}$. From the reference database, the two peaks were not present in the kaolinite mineral pattern suggesting that the kaolinite used in the study had some Halloysite to a smaller fraction. Kaolinite basal reflection was at 12.290° $d=7.196 \text{ \AA}$ and 24.805° $d=3.587 \text{ \AA}$. As compared to the reflection from the database these values agree in the d values suggesting that kaolinite was the major phase present in the clay mineral as presented in Table 3 and the minor phase of halloysite in Table 4.

Besides the phases present in the clay minerals, the crystallinity values were calculated. The original kaolinite sample was 75.0% crystalline and 25.0% amorphous. This shows that the kaolinite clay mineral was not fully crystalline as the 25% amorphous content showed the degree of the broken part of clay mineral present in the crystal lattice. The size of the background hump is shown in Figure 11. The background hump shows the total amorphous content of the phases present in the clay mineral. From the Figure 10 below, it is evident from the residue that resulted from exposing kaolinite to high temperature and high pressure in the presence of ultrapure water, there are no shifts in the peak position suggesting that no new phases were formed in the process. Also, the residue from kaolinite reacted under the same reservoir conditions in the presence of a saline environment of 1M sodium chloride; there was no evidence of shifts in the peaks positions as shown in Figure 10. However, on exposing kaolinite to the same reservoir conditions under strongly basic conditions of 1M potassium hydroxide, there is the creation of 3 new peaks in the process. An example of the peak formed was at 28.994° $d=3.077 \text{ \AA}$. This peak reflection was caused by halloysite. From the comparison of the XRD peaks from this study and those from the crystallographic database, it was found that many of the peaks present in the kaolinite clay mineral are caused by basal reflections of both kaolinite and halloysite. This was represented by the (K/H) standing for a shared peak position by kaolinite and halloysite as shown in the figure below. This made the identification of phases present in the residues using the XRD measurements difficult and thus additional information was required to confirm this.

Further characterization of the residue from the reaction of kaolinite with 1M potassium hydroxide revealed that kaolinite transformed to more of a halloysite phase. The number of crystalline proportions present in the solid minerals was determined. The original sample had a crystalline content of 75% and an amorphous content of 25% showing that the original sample was not fully crystalline. The changes in the crystallinity values showed that the original kaolinite sample reacted differently in line with the changes in the reagent. For example, on reaction with ultrapure water under high temperature and high pressure, the percentage crystallinity was 72.3, and the percentage amorphous was 27.3, and on reaction with 1M sodium chloride under high temperature and high pressure, the crystallinity values were 71.0% crystalline and 29.0% amorphous. From the reaction kaolinite with 1M potassium hydroxide, 55.0% was the crystalline value while 45.0% was the amorphous fraction. A table showing these crystallinity values is given in Table 5. The changes in these values show that geothermal reservoir conditions under near neutral

pH of approximately 7 and weak basic environments with a pH of 9 alter the kaolinite mineral as evidenced by the low deviations of crystallinity values of this environments from the original sample. However, strong basic environments of pH 14 do lead to alteration of the kaolinite mineral. The increase in the amorphous content evidenced that the kaolinite mineral under the strong basic conditions in presence of high temperature and pressure breaks down. Figure 11 shows the changes in the amorphous content from each experiment conducted by this study.

Table 3. Showing the d values and scan angles of the basal reflections attributed to kaolinite clay mineral from this study compared to the reference datasets from the ICDD database. The angle is the scan angle in degrees and the d value is the 2-theta position in Angstrom.

This study		Reference Kaolinite one		Reference Kaolinite two	
Angle (°)	d Value (Å)	Angle (°)	d Value (Å)	Angle (°)	d Value (Å)
12.290	7.196	12.363	7.154	12.365	7.153
24.805	3.587	24.873	3.577	24.877	3.576

Table 4. Showing the d values and scan angles of the basal reflections attributed to halloysite clay mineral from this study compared to the reference datasets from the ICDD database. The angle is the scan angle in degrees and the d value is the 2-theta position in Angstrom.

This study		Reference halloysite	
Angle (°)	d Value (Å)	Angle (°)	d Value (Å)
8.783	10.060	8.753	10.094
17.669	5.016	17.558	5.047
28.994	3.077	28.681	3.110
42.340	2.133	42.302	2.135

Table 5. Showing the crystallinity values of each reaction from the experiment conducted with kaolinite mineral where %C is the percentage change in crystalline content and %A is the percentage in amorphous content. The Kao.OD.XRD is the original oven dried material, Kao.W.R.XRD is kaolinite reacted with Ultrapure water, Kao.N.R.XRD is kaolinite reacted with 1M sodium chloride and Kao.K.R.XRD is kaolinite reacted with 1M potassium hydroxide.

Kaolinite	%C	%A
Kao.OD.XRD	75.0	25.0
Kao.W.R.XRD	72.3	27.7
Kao.N.R.XRD	71.0	29.0
Kao.K.R.XRD	55.0	45.0

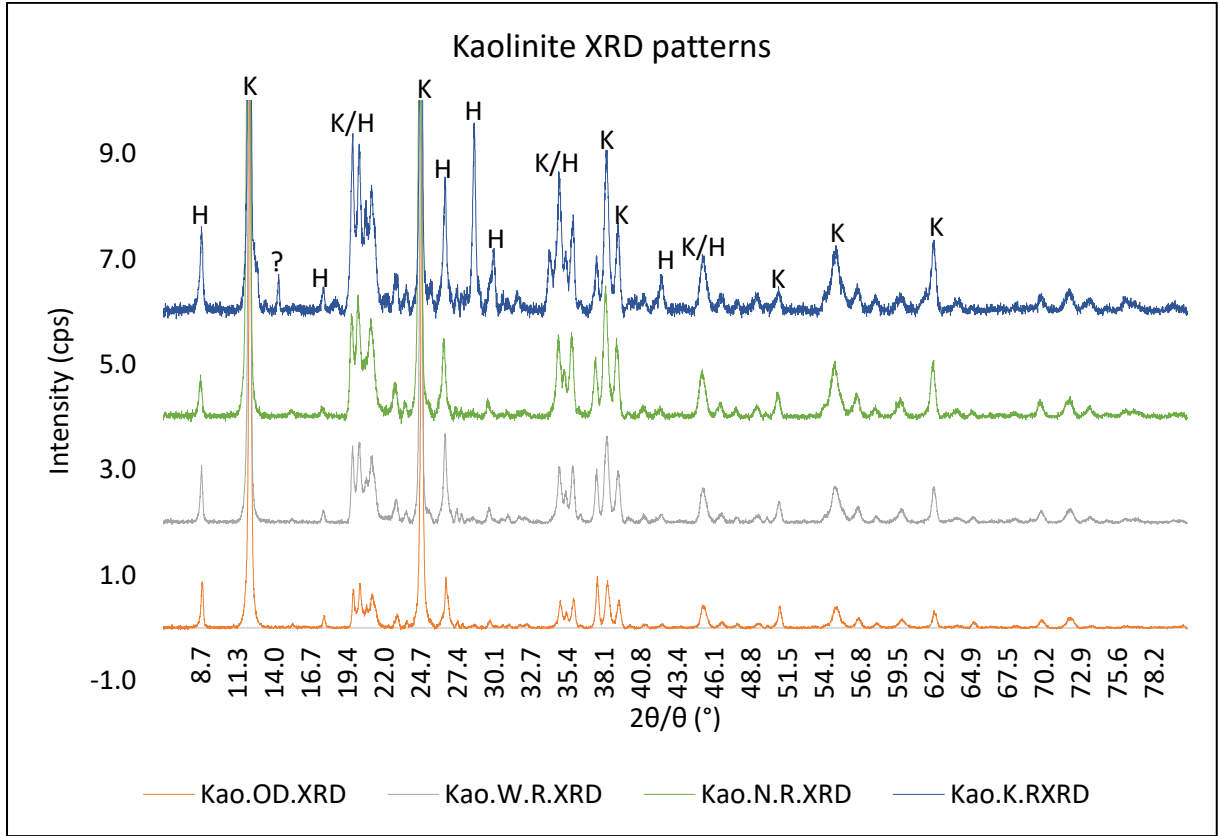


Figure 10. Background subtracted XRD patterns of kaolinite showing various peaks positions and intensities. The patterns were stacked in the order of +2 for kaolinite reacted with ultrapure water(Kao.W.R.XRD) and +4 for kaolinite reacted with 1M sodium chloride(Kao.N.R.XRD) and +6 for kaolinite reacted with 1M potassium hydroxide(Kao.K.R.XRD) to enhance visibility of each individual pattern. The intensity scale range was set between 1 and 10 for small peak visibility. H are the peaks caused by halloysite while K are the peaks caused by kaolinite. Cps stands for counts per second. The question marks refer to a peak that was not identified.

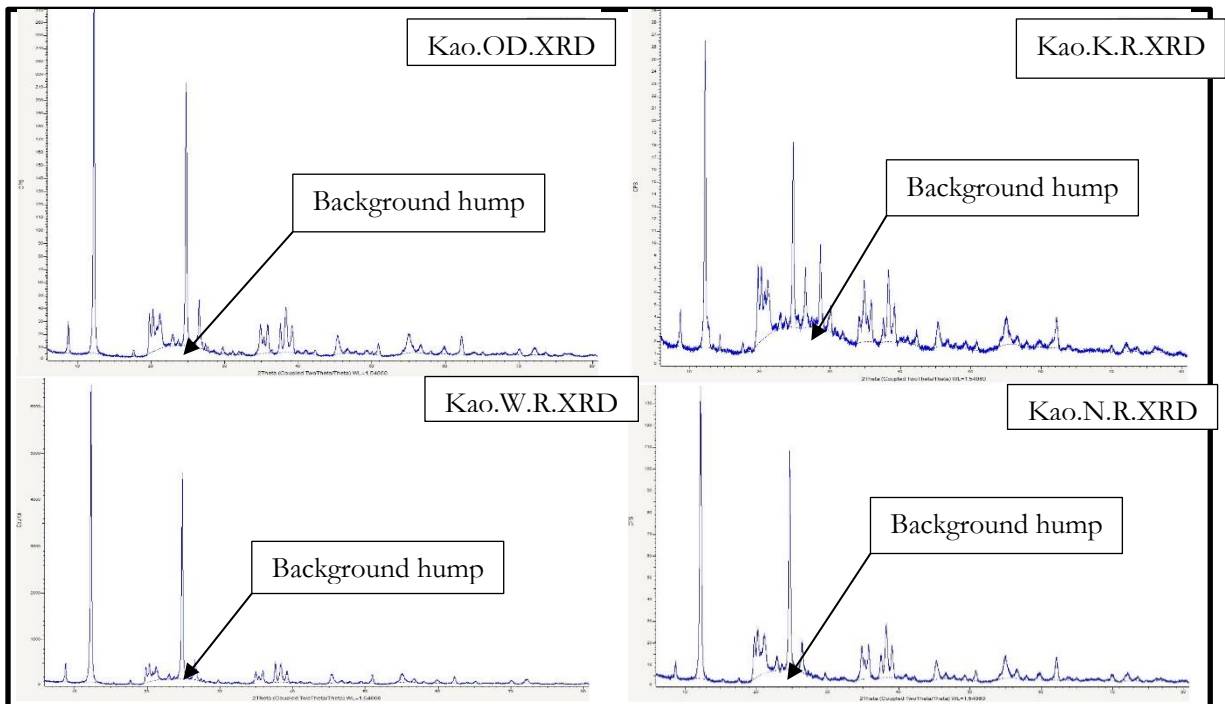


Figure 11. Original+background XRD patterns of Kaolinite showing the changes in the background hump in relation to the various environments exposed to. The patterns show original sample(Kao.OD.XRD), Kaolinite

reacted with ultrapure water(Kao.W.R.XRD), kaolinite reacted with 1M sodium chloride(Kao.N.R.XRD) and kaolinite reacted with 1M potassium hydroxide(Kao.K.R.XRD).

Montmorillonite was the only phase present in the clay mineral used and a result of exposing it to high pressure and high temperature under varying pH conditions, the peak positions and intensities remained unchanged except for the creation of new peaks in presence of strong basic conditions as shown in Figure 12.

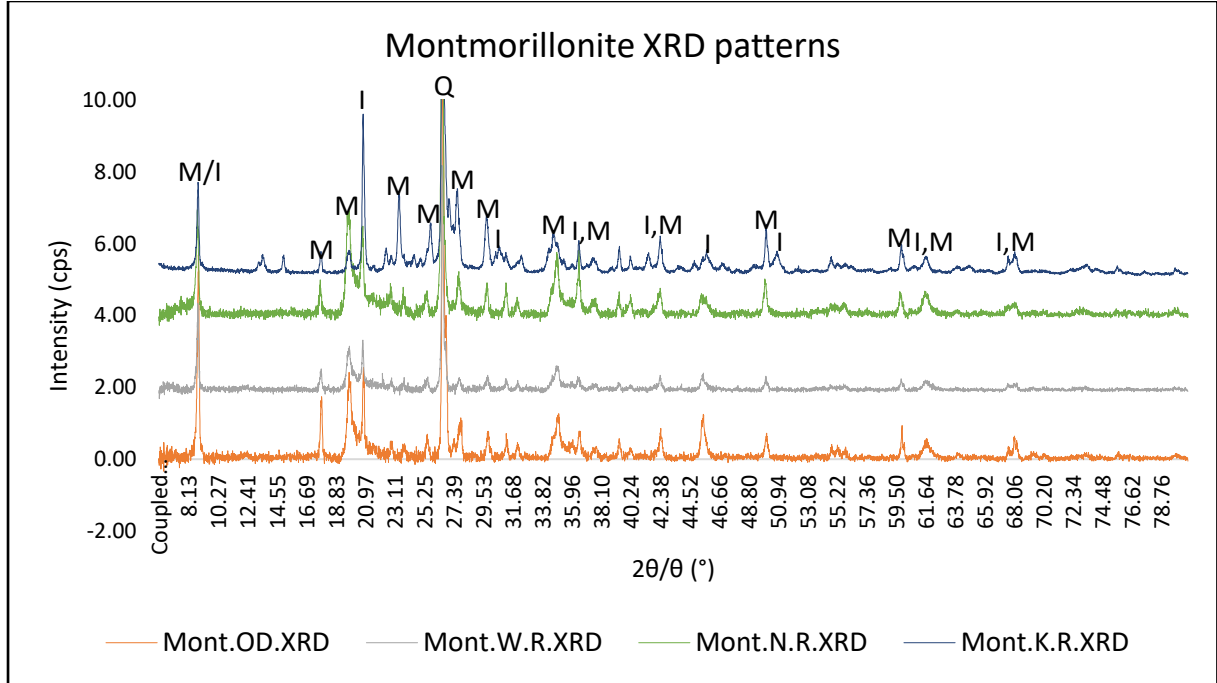


Figure 12. Background subtracted XRD patterns of montmorillonite residues from reaction with ultrapure water(Mont.W.R.XRD), 1M sodium chloride (Mont.N.R.XRD), and 1M potassium hydroxide(Mont.K.R.XRD). The patterns were stacked in the order of +2 for montmorillonite reacted with ultrapure water and +4 for montmorillonite reacted with 1M sodium chloride and +5 for montmorillonite reacted with 1M potassium hydroxide to enhance visibility of each individual pattern. The intensity scale was set to values between -2 and 10 to show the various peaks intensities. M denotes basal reflections caused by montmorillonite, Q denotes basal reflections caused by quartz and I denotes reflections caused by illite. Cps stands for counts per second

From further comparison of the scan from this study with the peaks from the crystallographic database, this study was able to find out that illite was the most potential phase present in the residue. This conclusion was reached after comparing the number of peaks from the residues under study that coincide with the illite phase from the crystallographic database. The characteristic peaks for montmorillonite found by this study was at the 8.85° $d=9.98\text{\AA}$ as the first basal reflection while the second basal reflection is at the 17.80° $d=4.98\text{\AA}$, the third peak was at 19.67° $d=4.51\text{\AA}$, the fourth peak at 19.79° $d=4.48\text{\AA}$ as shown in Table 6. The most intensive peak was at the 26.64° with a 100% intensity. This reflection was influenced by quartz. Quartz has peaks at 26.63° $d=3.34\text{\AA}$, 36.5° $d=2.43\text{\AA}$ and 39.4° $d=2.28\text{\AA}$. Table 7 shows the characteristic peaks caused by illite. The Figure 12 above shows these peak positions suggesting the presence of quartz in the samples. Other researchers have found that such reflection of quartz is indicated by the reflection at the 26.6° (Fatimah, Wang, Narsito, & Wijaya, 2010). Montmorillonite shows reflections at 6.3° , 19.89° and 35.6° (Fatimah, Shaobin, & Dessy, 2011). The characteristic reflections of montmorillonite occur at 15.15\AA and 4.50\AA (Shahwan, Erten, & Unugur, 2006). Montmorillonite XRD patterns show characteristic reflections at 6.3° , 19.9° , 21.8° , 19.80° , 34.96° and 26.64 (Tabak, Afsin, Aygun, & Icbudak, 2005).

Table 6. Showing the d values and scan angles of the basal reflections attributed to Montmorillonite clay mineral from this study compared to the reference datasets from the ICDD database. The angle is the scan angle in degrees and the d value is the 2-theta position in Angstrom.

This study		Reference Montmorillonite	
Angle (°)	d Value (Å)	Angle (°)	d Value (Å)
8.850	9.980	9.124	9.685
19.670	4.510	20.645	4.299
19.790	4.480	26.672	3.334

Table 7. Showing the d values and scan angles of the basal reflections attributed to Illite clay mineral from this study compared to the reference datasets from the ICDD database. The angle is the scan angle in degrees and the d value is the 2-theta position in Angstrom.

This study		Reference Illite	
Angle (°)	d Value (Å)	Angle (°)	d Value (Å)
8.850	9.983	8.816	10.022
26.614	3.347	26.604	3.347
31.209	2.864	31.171	2.867

Reaction of montmorillonite with ultrapure water and 1M sodium chloride under geothermal reservoir conditions show no phases changes in the overall clay mineral. This is evident from the little variations of the XRD patterns of these experiments from the original unreacted montmorillonite clay mineral pattern. A further analysis was done on the crystallinity of the montmorillonite clay mineral and from the results it was found that the original montmorillonite clay mineral had a crystallinity percentage of 50.4 and an amorphous content of 49.6%. Montmorillonite reacted with ultrapure pure water was 49.0% crystalline and 51.0% amorphous. The reaction between 1M sodium chloride and montmorillonite lead to a residue that was 49.7% crystalline and 50.3% amorphous. The residue from the experiment of montmorillonite and 1M potassium hydroxide was 75.5% crystalline and 24.5% amorphous. Table 8 below shows values for each experiment conducted by this research.

Table 8. Showing the crystallinity values of each reaction from the experiment conducted with Montmorillonite mineral where %C is the percentage change in crystalline content and %A is the percentage in amorphous content. The Mont.OD.XRD is the original oven dried material, Mont.W.R.XRD is Montmorillonite reacted with Ultrapure water, Mont.N.R.XRD is Montmorillonite reacted with 1M sodium chloride and Mont.K.R.XRD is Montmorillonite reacted with 1M potassium hydroxide.

Montmorillonite	%C	%A
Mont.OD.XRD	50.4	49.6
Mont.W.R.XRD	49.0	51.0
Mont.N.R.XRD	49.7	50.3
Mont.K.R.XRD	75.5	24.5

The variations from the original sample by the reaction between ultrapure and 1M sodium chloride was insignificant to say there was a change in these environments. This shows that such neutral and weak basic environments did not alter the montmorillonite mineral unlike the strong basic environments. From the XRD data, the changes in the background which is due to the total amorphous content in the clay mineral phases present was also conducted. The montmorillonite phase shows that the amorphous content of the final residue decreased compared to the original material. This shows that montmorillonite on reaction

with strong basic environments gets well-ordered because potassium hydroxide is a swelling inhibitor and thus reduces the mobility of cations thus increasing the compactness of the clay mineral (Miao et al., 2017). These changes are shown in Figure 13. The X axis scale is counts per second and the Y axis scale is the coupled two theta over theta. The main purpose of the diagram was to show the changes in the background hump during the various experimental stages. An example shown is the one from the reaction of montmorillonite with 1M potassium hydroxide where the background hump was almost gone, and this is also supported by the decrease in the amorphous content from 49.6% to 24.5%. Therefore, this study argues that clay caprocks closed via montmorillonite clays under reservoir conditions simulated by this study do not get altered in neutral to weak basic solutions while under strong basic solutions it gets altered and well ordered.

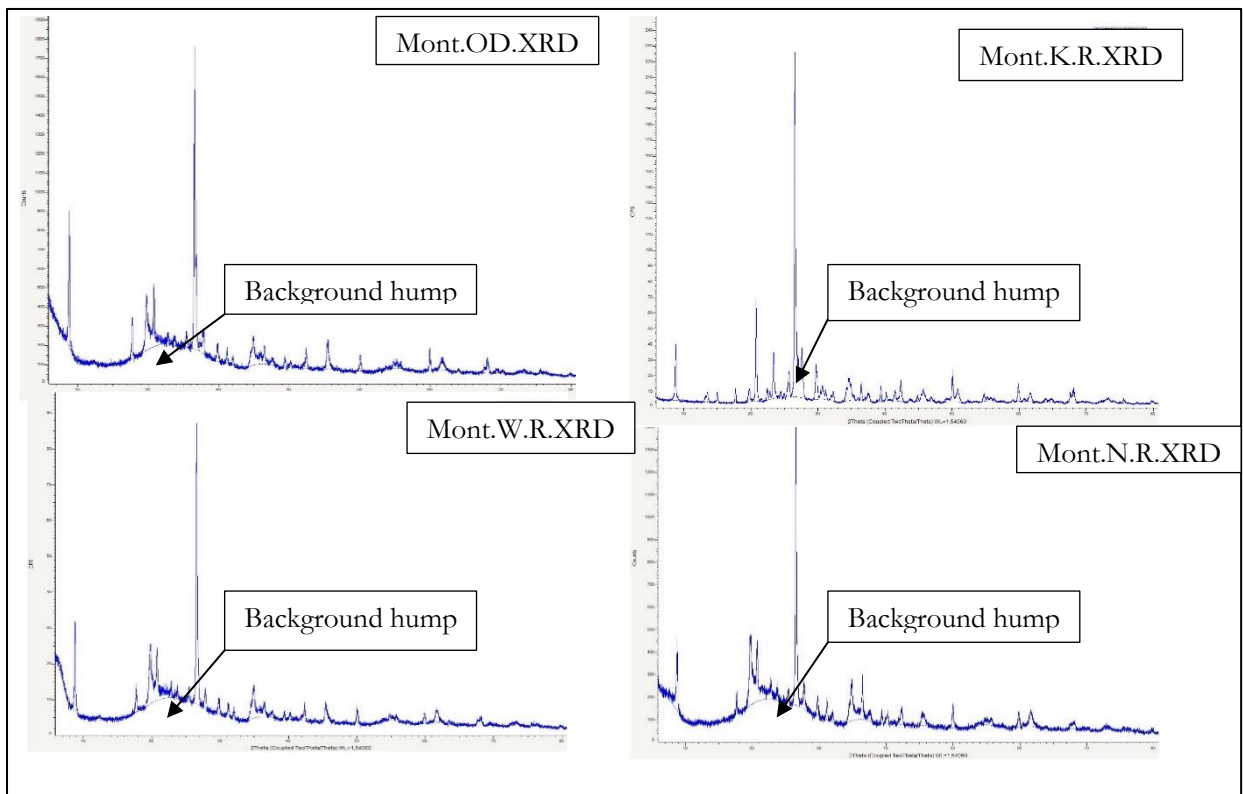


Figure 13. Original + background XRD patterns of Montmorillonite showing the changes in the background hump in the different stages of the experiment where Mont.OD.XRD refers to the original sample, Mont.W.R.XRD refers to the residue from reaction with ultrapure water, Mont.N.R.XRD refers to residue from reaction with 1M sodium chloride and Mont.K.R.XRD refers to residue from reaction with 1M potassium hydroxide.

5.2. ASD Result

From characterization using the ASD, the spectra showed the presence of kaolinite in the original oven dried sample. This conclusion was arrived at after comparing the spectra from this study with those from the USGS spectral library. However, due to differences in the measuring device wavelength scale range, it was not possible to overlay all the spectra from this research and those from the USGS in one spectral plot. From Figure 14 below it was evident that the original sample was kaolinite. This was shown by the characteristic doublets in the 1400nm feature and the 2200nm feature. For kaolinite also, the depth of the 1900nm absorption feature is small. On comparison with the USGS spectral plots the kaolinite in this study is like the one from the USGS spectra library as shown in Figure 15. The reaction of kaolinite with ultrapure water and 1M sodium chloride show no much variations from the original sample. The absorption features do not get altered in the process. However, on reaction with 1M potassium hydroxide

the left asymmetry of the 1400nm absorption feature, which is caused by water and OH, becomes deeper. As compared to the other spectra it showed an increase in the water content in this region. The 1900nm absorption feature of kaolinite, caused by water, on exposing to 1M potassium hydroxide also showed an increase in depth compared to the other experiments. The characteristic doublets in the 2200nm feature, caused by Al-OH, dip to the longer wavelengths and thus resemble kaolinite and on reacting with 1M potassium hydroxide this shoulder flattened unlike the other residues from the experiment. This showed that there were no phase changes in the two reacted spectra but the residue from the experiment with 1M potassium hydroxide showed a new phase. From comparison with the spectra from the USGS spectral library the new phase was halloysite as shown in Figure 15. The vibrations caused by metal hydroxides i.e. (Fe, Mg)-OH remain unaffected in the entire experimental runs. Research has shown that due to breaking of the OH bond kaolinite transforms to metakaolin at temperatures between 400-800°C (Mechri, Chihi, Mahdadi, & Beddiaf, 2017). This study used temperatures of below 250°C and thus the transformation could not be evident in the residues. However, kaolinite can also transform to a reactive amorphous phase through thermal activation (-Amin, Alam, & Gul, 2014).

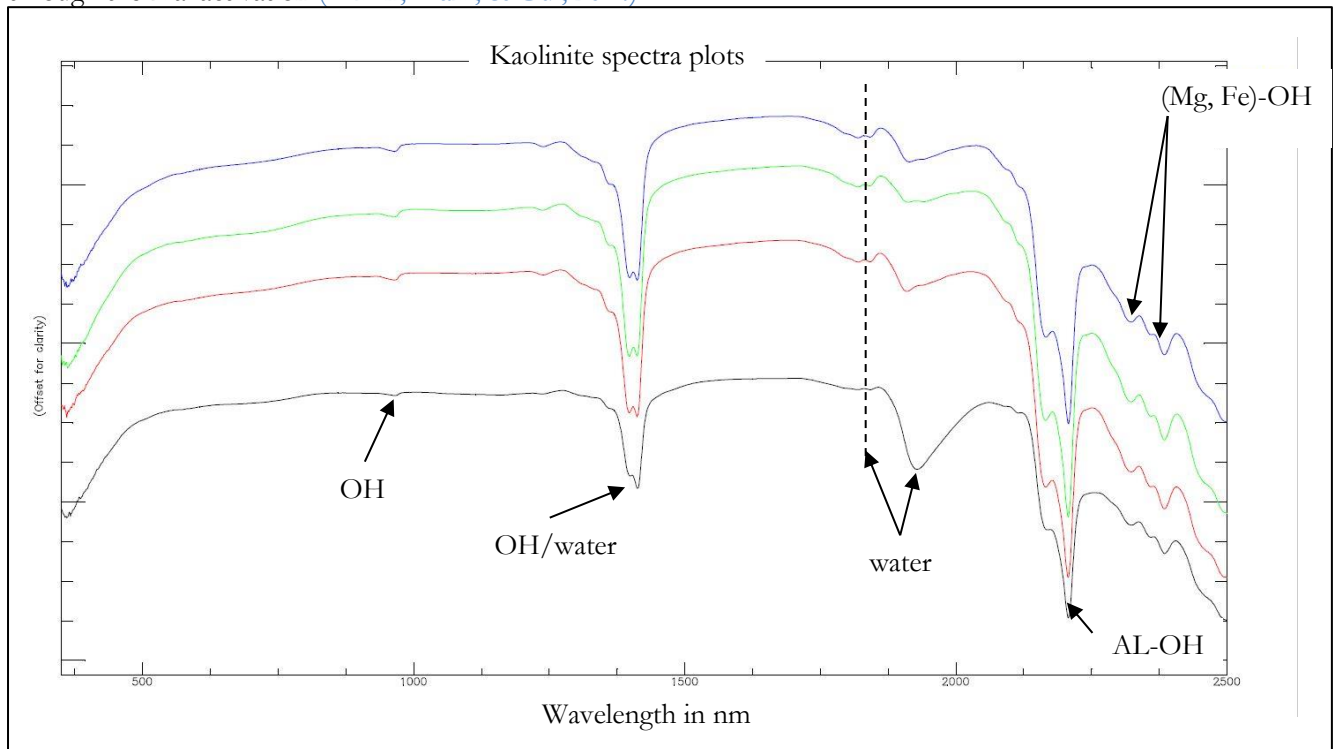


Figure 14. Diagram showing the Stacked kaolinite ASD spectra from this study where the colors; blue represents Kao.OD.ASD, green represents Kao.W.R.ASD, red represents Kao.N.R.ASD and black-Kao.K.R.ASD. The reflectance values were offset for clarity.

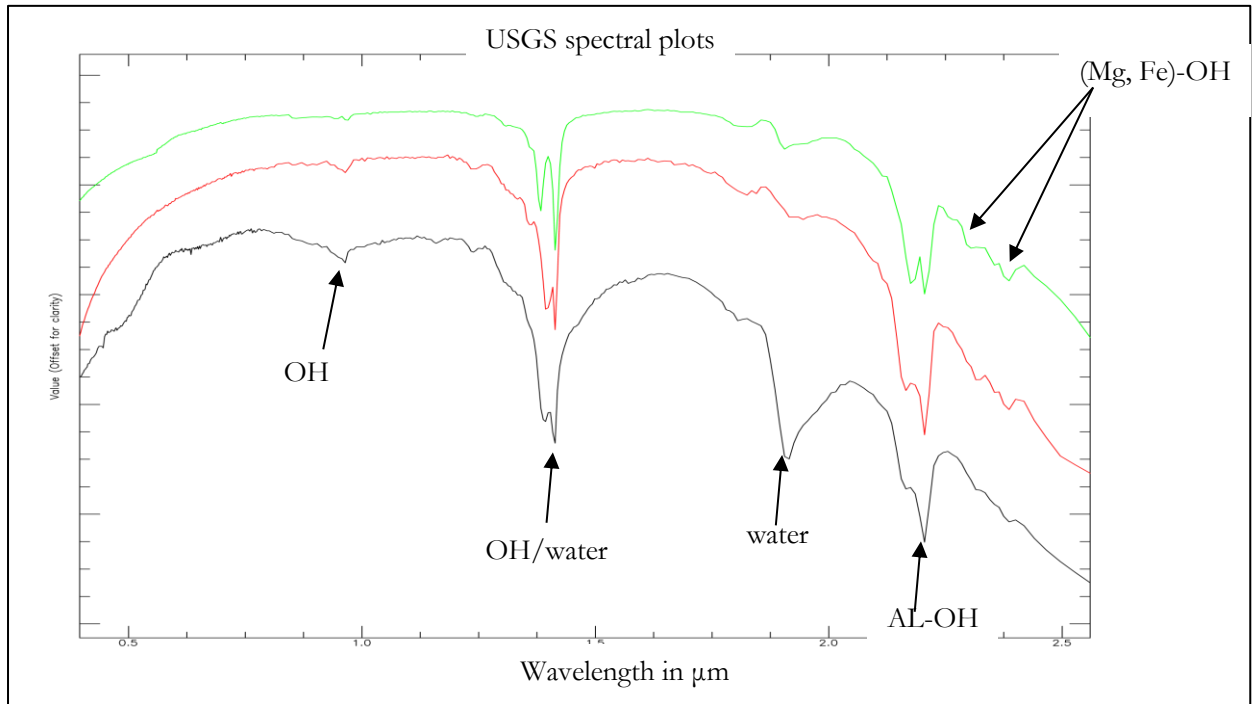


Figure 15. diagram showing Stacked ASD spectra from the USGS spectral library showing Dickite(green), Kaolinite(red) and Halloysite(black). The reflectance values are offset for clarity, while the x axis values are the wavelength in micrometres.

To calculate for the crystallinity variations, the four spectra were zoomed to the Al-OH feature between 2160nm and 2200nm, and this was used to calculate the crystallinity of kaolinite as shown in Figure 16. The position of the absorption feature used is illustrated below, and this reflectance values recorded in Table 11 provide in Appendix 2. The crystallinity of unreacted kaolinite was 0.990 while that of kaolinite reacted with ultrapure water was 0.988, kaolinite reacted with 1M sodium chloride was 0.989 and kaolinite reacted with 1M potassium hydroxide was 0.975. From previous research, it is stated that kaolinite with a crystallinity of less than one is usually considered disordered (García, Vigil De La Villa, Vegas, Frías, & Sánchez De Rojas, 2007). The values from this research agree with this hypothesis as all the values for crystallinity from the table are below one and thus decreases further away from one. The values of the original sample, ultrapure water and 1M sodium chloride showed that the clay mineral was not affected much by the reagents in the simulated reaction process. The decrease in crystallinity in reaction with 1M potassium hydroxide supports the XRD data of an increase in the amorphous content. This shows that kaolinite broke down in the presence of high basic solutions. The presence of halloysite in the original kaolinite clay can be attributed to the low crystallinity values of below 1. The previous study has reported that well-ordered kaolinite has values above 1 (García et al., 2007). From Figure 16 below it is evident that the kaolinite shoulder in the 2200 nm characteristic doublet disappears in the residue from reaction with 1M potassium hydroxide. This result further supports the XRD crystallinity values of kaolinite mineral breaking down and increasing in the amorphous content.

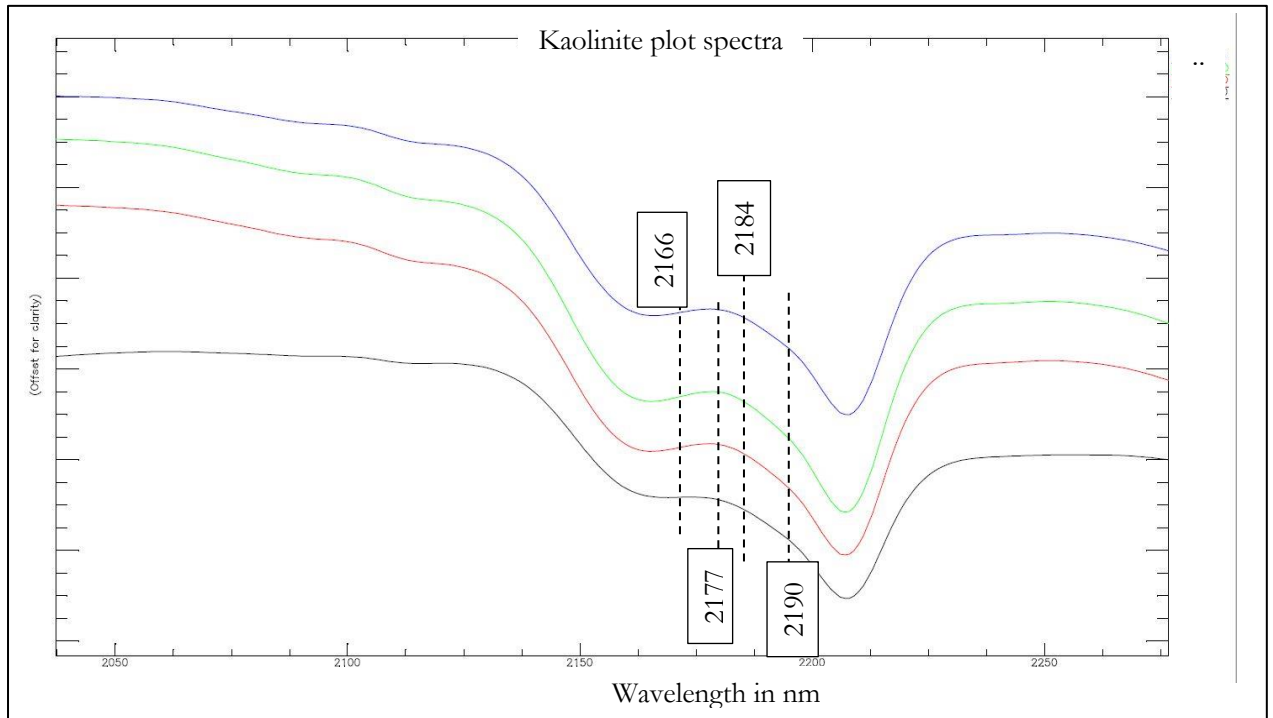


Figure 16. Zoomed out spectra of Stacked Kaolinite ASD spectral range (2100-2250) nm of the values used to calculate crystallinity where; blue is Kao.OD.ASD, green is Kao.W.R.ASD, red is Kao.N.R.ASD and black are Kao.K.R.ASD. The values written down are the points as to which the reflectance values were used to calculate crystallinity in the equation the reflectance values are offset for clarity.

The presence of prominent 1900nm features makes the crystallinity characterization of montmorillonite different from kaolinite. The ratio of the 2200nm and the 1900nm depth features were used to determine the crystallinity of montmorillonite. The stacked spectral plots of montmorillonite shown in Figure 17 shows little variations while experimenting with ultrapure water and 1M sodium chloride. The spectra plot on comparison with the spectral plots from the USGS spectral library is all montmorillonite. Changes or deviations from the original material begin to be noticed in reaction with 1M potassium hydroxide. The depth of the absorption features decreases, and the shoulders also disappear as shown in Figure 17 below. The shape of the spectra is also different from the other spectra. From comparison with the USGS spectral library plots, this study was able to determine that a new phase was formed in reaction 1M potassium hydroxide under epithermal conditions. The new phase formed was illite. Illite has additional absorption bands in the 2350nm and 2450nm unlike montmorillonite (R. N. Clark et al., 1990). This feature is related to Al-OH. However, the 2450nm feature of Illite is weakly defined as shown in Figure 18. This result is also supported by the XRD patterns as there was an increase in the peaks due to the basal reflections caused by Illite. The total crystallinity calculated from the XRD pattern is also in agreement with this statement as the total crystallinity of the residue from 1M potassium hydroxide is up by over 20% compared to the original sample. Muscovite almost lacks an absorption feature in 1900nm position, and thus it was not considered. Due to variations in the equipment wavelength scale range used to collect the spectra from the USGS, this study was not able to overlay each of the spectra from this research and that of the USGS in one spectra plot. This research, therefore, argues that given a geothermal reservoir condition, montmorillonite transforms to Illite in the presence of strong basic environments. montmorillonite for this study shows that given high temperature and high pressure under near neutral to weak basic solutions shows no degree of change in phase and thus it can further be argued that such conditions do not have a dire effect on the said clay mineral. However, this study simulated reservoir conditions for 6 days and thus the effect of time is subject to further study.

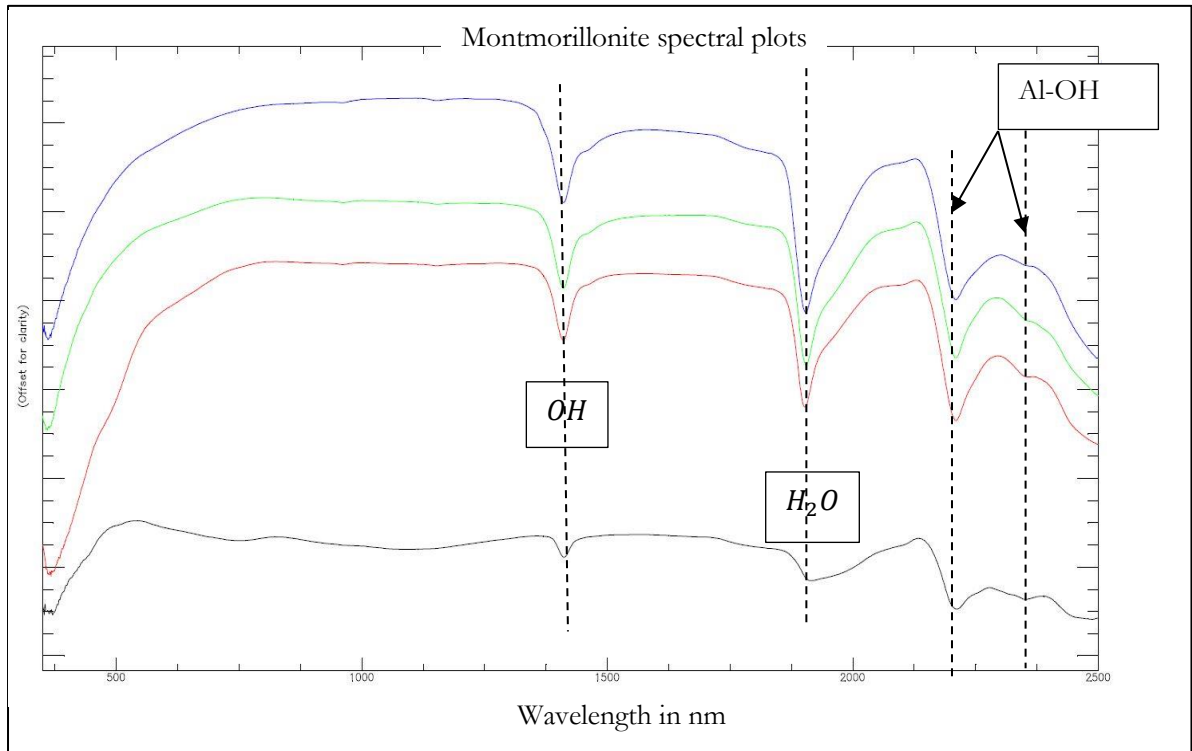


Figure 17. Showing stacked ASD spectra of Montmorillonite from this study showing the absorption feature positions where; blue is Mont.OD.ASD, green is Mont.W.R.ASD, red is Mont.N.R.ASD and black is Mont.K.R.ASD. The reflectance values were offset for clarity.

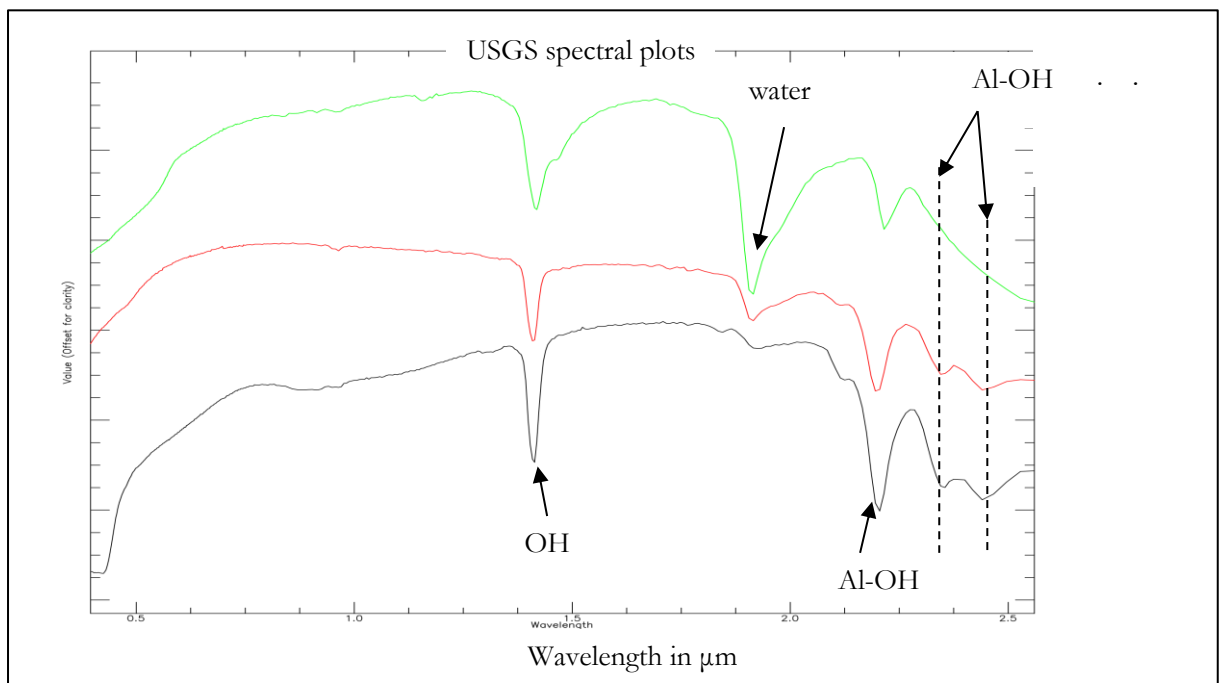


Figure 18. Diagram showing Stacked ASD spectra of Montmorillonite from the USGS spectral library where; green is Montmorillonite, red is Illite and black is Muscovite. The reflectance values were offset for clarity.

One of the features required to calculate the crystallinity of montmorillonite is the 1400nm asymmetry and to extract this feature the spectra plots were viewed in ENVI IDL DISPEC. This calculates the asymmetry of this feature after removing continuum as shown in Figure 19. The values of the 1400nm feature used by this study are given in Table 12 as appendix 2.

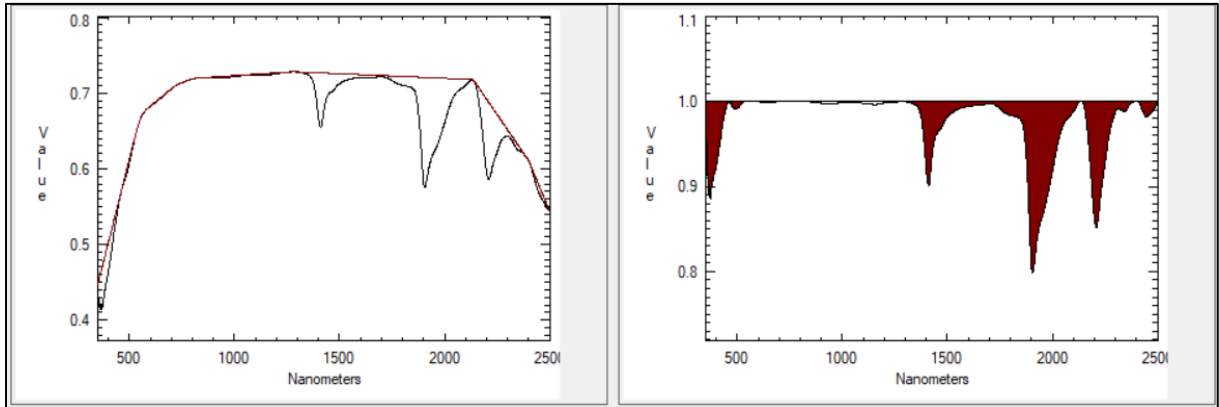


Figure 19. Spectra plot showing a continuum removed spectra of Montmorillonite in IDL DISPEC used to calculate the asymmetry of the 1400nm absorption feature used to calculate the crystallinity index of Montmorillonite. The values of the reflection extracted from the spectra are listed in appendix 2.

The other features required to calculate the crystallinity of montmorillonite is the ratio of the 2200D/1900D. Zoomed spectra of this features are shown in Figure 20. The values show the position to which the reflectance measurements were extracted from. From the equation including these parameters, the crystallinity of original montmorillonite was 1.231, montmorillonite reaction with ultrapure water was 1.171, montmorillonite reaction with 1M sodium chloride was 1.146 and montmorillonite reacted with 1M potassium hydroxide was 1.055. This shows that the crystallinity variations in montmorillonite drop in the ASD data though the XRD results show an increase in the overall crystallinity, i.e. the crystallinity of the whole mineral phase. The values that were extracted and calculated are provided in appendix 3 as Table 12. The general decreasing trend in the crystallinity variations can be attributed to the decrease in the depth of the absorption features that were used in the calculation of crystallinity. The 2200 absorption feature is often considered as an indicator of aluminum content (Duke, 1994; van Ruitenbeek et al., 2005). As crystallinity is calculated based on the ratio of reflectance of the positions, therefore the shift of this feature to longer wavelength is an indicator of poorly ordered structures. Aluminium rich minerals have the 2200nm feature in shorter wavelengths (Garcia, 2013)

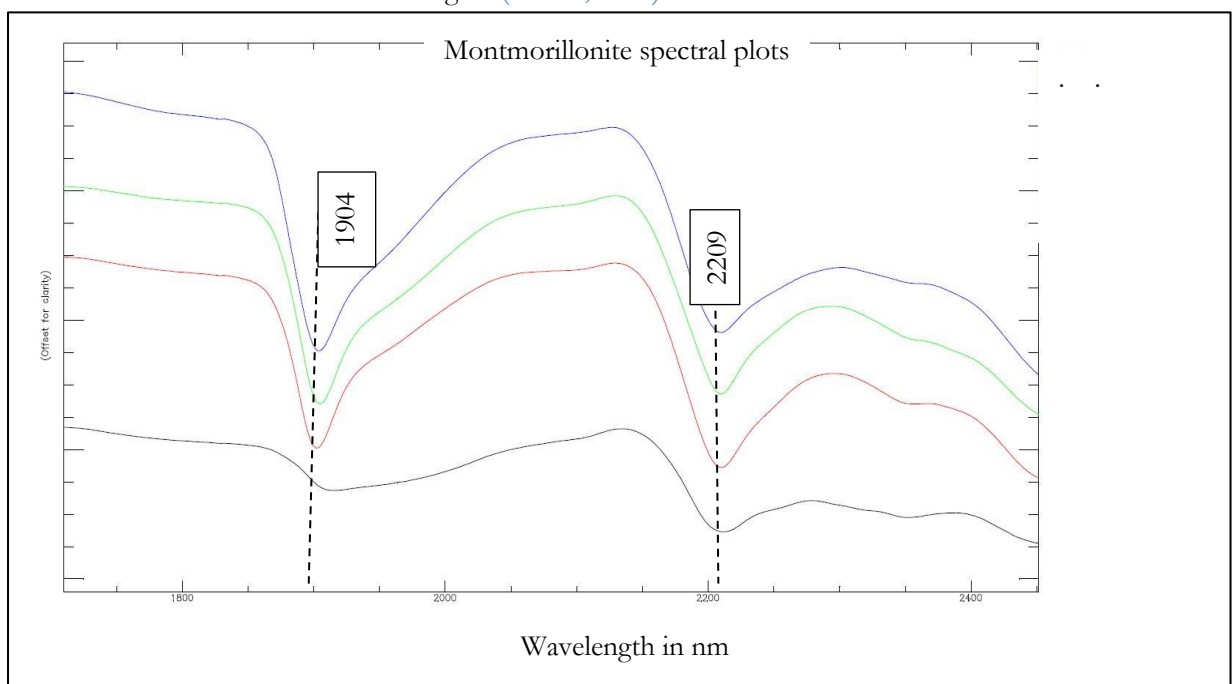


Figure 20. Zoomed spectra plot showing red -Montmorillonite reacted with 1M Sodium chloride(Mont.N.R.ASD), blue -original Montmorillonite(Mont.OD.ASD), green -Montmorillonite reacted with Ultrapure water(Mont.W.R.ASD), and black -Montmorillonite reacted with 1M potassium hydroxide(Mont.K.R.ASD). The positions stated are the ones as to which the reflectance values in the 1900nm and the 2200nm absorption feature were used to calculate the crystallinity of Montmorillonite. The values extracted are given as a table in Appendix 2.

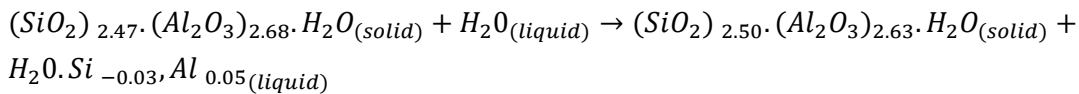
5.3. ICP OES Result

From digestion of the original kaolinite sample, the formulae below was found

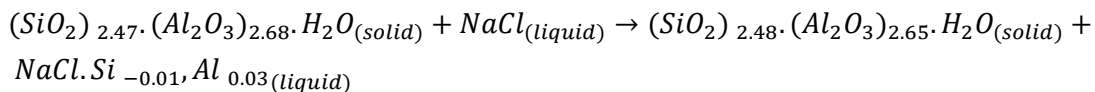
$(SiO_2)_{2.47} \cdot (Al_2O_3)_{2.68} \cdot H_2O$. The ions used were rounded off to two decimal places and thus elements like iron, calcium and magnesium were off the value. The presence of traces of Iron, Calcium and Magnesium in the clay mineral also suggests that the clay mineral was not purely kaolinite. These elements were present in the original clay sample as recorded by the ICP OES concentration. Montmorillonite sample had the following elemental percentage concentration of

$(SiO_2)_{5.42} \cdot (Al_2O_3)_{1.23} \cdot (Fe_2O_3)_{0.11} \cdot (CaO)_{0.01} \cdot (MgO)_{0.13} \cdot H_2O$. From ICP OES analysis it was evident that the blank fusion had higher concentration of Na and K and thus suggesting that these elements were not present in the clay mineral composition of both kaolinite and montmorillonite. Some traces of potassium were found in the reaction experiment with 1M potassium hydroxide. The residues were not washed. To this effect, this research argues that the presence of the potassium element in the residues from this experiment could be as a result of addition of potassium hydroxide reagent but whether the element formed part of the clay mineral lattice or it was just a crystal was not determined. The ionic values used in the recalculation of the chemical formulae of the original sample and the residues from each experiment are given in Table 9 and Table 10.

Equations derived were based on the reactants and the products from the experiments. The reaction with ultrapure water, for example, shows that Si and Al were broken down. However, there was no new phase formed in the reaction process as shown below.



The reaction between kaolinite and 1M sodium chloride did not also lead to a new phase and thus represented by the reaction equation below. The number of ions Si and Al show some changes.



A reaction between kaolinite and 1M potassium hydroxide lead to the breakdown of kaolinite to halloysite as shown in the reaction equation below. This research did not account for water present in the clay mineral and thus provided the equation below.

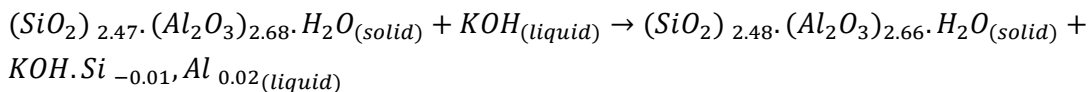


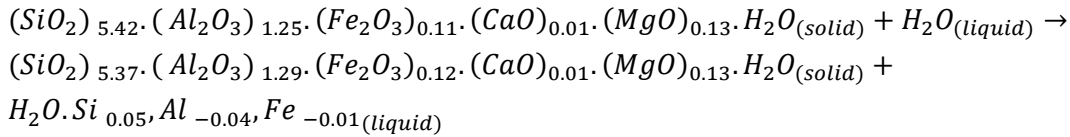
Table 9. A table showing the number of ions in the formula for each element present in each Kaolinite both the original and residue calculated from the total amount in concentration. Where Mg is magnesium, Ca is calcium, Fe is iron; Al is aluminum, Si is silica. Kao.OD stands for original oven dried Kaolinite sample, Kao. W. R is the residue from the experiment with ultrapure water, Kao. N. R is the residue from the experiment with 1M sodium chloride, Kao. K. R is the residue from the experiment with 1M potassium hydroxide.

	Mg	Ca	Fe	Al	Si
--	----	----	----	----	----

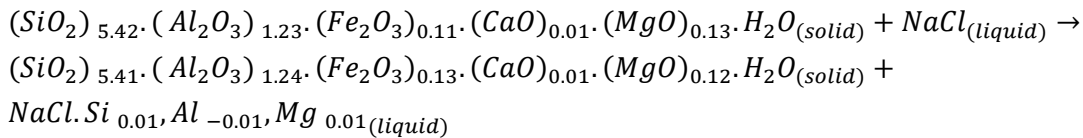
Kao.OD	0.00456	0.00196	0.0194	2.68	2.47
Kao. W. R	0.00721	0.00174	0.0272	2.63	2.50
Kao. N. R	0.0100	0.00100	0.0260	2.65	2.48
Kao. K. R	0.0102	0.00228	0.0242	2.66	2.48

At shorter reaction times, of temperature and high potassium hydroxide concentrations, total dissolution of kaolinite can be reached (Alberto, Reyes, & Williams, 2010). Kaolinite reaction with alkaline solutions leads to the release of Silica and Aluminium (Zhao, Deng, Harsh, Flury, & Boyle, 2004). This works from other studies also support the results from this study where some moles were dissolved by the strong basic environment.

Montmorillonite reaction with ultrapure water showed that the clay mineral was not altered much like the residue from the experiment was montmorillonite as shown in the reaction below.



Hydrothermal simulation of reservoir brine using 1M sodium chloride in reaction with montmorillonite also suggested that the montmorillonite clay mineral phase was not altered in the process. The reaction equation for the experiment was as shown below.



The montmorillonite reaction with 1M potassium hydroxide leads to the formation of a new illite phase. The reaction equation that took place was as shown below. From the equation, it is evident that there is an increase in the elements in the residue compared to the original. This was because of the heating in the presence of potassium hydroxide which is a swelling inhibitor thus solidifying the mineral resulting in a phase change to illite. Also, the Tschermack substitution played a role in the fixation of Al and Si in the reaction process.

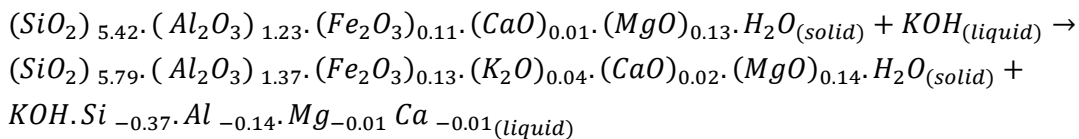


Table 10. Showing the number of ions for each element present in each Montmorillonite, i.e. both the original and the residue calculated from the total amount in concentration. Where Mg is magnesium, K is potassium, Ca is calcium, Fe is iron, Al is aluminum, Si is silica. Mont.OD stands for original oven dried Montmorillonite sample, Mont. W.R is the residue from the experiment of Montmorillonite with ultrapure water, Mont. N.R is the residue from the experiment of Montmorillonite with 1M sodium chloride, Mont. K.R is the residue from the experiment of Montmorillonite with 1M potassium hydroxide.

	Mg	Ca	K	Fe	Al	Si
--	----	----	---	----	----	----

Mont.OD	0.134	0.0142	-	0.114	1.23	5.42
Mont. W. R	0.127	0.0126	-	0.119	1.29	5.37
Mont. N. R	0.120	0.0694	-	0.134	1.24	5.41
Mont. K. R	0.135	0.0168	0.0414	0.126	1.37	5.79

From all the experiments that were conducted by this research, a residue and filtrate were the final products resulting from separation from the solution after the experiment. However, using a calibration line of 0.000 $\mu\text{g/g}$ to 100 $\mu\text{g/g}$, it was not easy to determine the concentration of elements in the solution because the concentration values from the ICP measurement were above the calibration line of 100 $\mu\text{g/g}$. To correct for the values above the calibration line, a dilution of the filtrate was required. However, after the first ICP measurement, the liquid left was not enough to run another measurement on all of the filtrates. Much of the liquid fraction was lost in the process of filtration, and thus this determined the final concentration of the elements present in the filtrate which served as an idea to understanding what was leaching out of from the clay minerals that had been through the experiment difficult. In a typical geothermal plant, the amount of the total dissolved solids present in geothermal waters are usually an indicator of dissolution of minerals in deep down in the reservoir.

The original sample and the residues from each experiment were digested to understand what the difference between the original sample and the residues for each clay mineral was used in this study. The analysis showed that the original material had a higher concentration of all elements while the strong basic environment has the least concentration of each element studied by this research for the kaolinite mineral. This variation in the individual experiment concentration shows that given different environments the stability of the minerals is greatly affected. This study further argues that kaolinite mineral is much affected by hydrothermal alteration compared to montmorillonite. Table 10 above shows that montmorillonite reacted under strong basic environments leads to fixation of the element and thus a higher number of ions compared to the original sample. The most affected elements are aluminum and silica. The presence of potassium ion in the residue of the experiment of montmorillonite and 1M potassium hydroxide further goes ahead to support other data from this experiment of a new illite phase formed because of the hydrothermal process. From the changes in the mineralogical compositions as shown in the equations above, this study argues that reservoirs closed off via kaolinite in the clay cap rock are prone to dissolution. Therefore, elements can migrate as fines up from deep down in the reservoir to the wellhead, and due to changes in temperature, these elements can precipitate out of the solution leading to scaling effect in the delivery pipes. However, determining the scaling effect and precipitation of minerals due hydrothermal alteration was beyond the scope of this study.

6. CONCLUSION AND RECOMMENDATION

In summary, this study was able to find out that kaolinite was not affected much by hydrothermal conditions in the presence of near neutral to weak basic conditions, i.e., ultrapure water and 1M sodium chloride as no new phases are formed although there is evidence of some breakdown of the clay mineral. kaolinite in reaction with 1M potassium hydroxide decreases in crystallinity and transforms to halloysite. All the experiments were conducted at a temperature of approximately 245°C and an average pressure of 233 bars.

Montmorillonite in the presence of 1M potassium hydroxide gets well-ordered and increases in crystallinity to illite. In the presence of ultrapure water and 1M sodium chloride, the clay mineral was not affected much as evidenced by the crystallinity values. The same pressures and temperatures used in kaolinite were used in the experiments conducted using montmorillonite.

Also, this study was able to conclude that it is possible to maintain a system under high temperature and high pressure in the laboratory. Therefore, this research was able to mimic a geothermal reservoir condition in the laboratory using high temperature and high pressure with changes in pH and since the number of factors affecting the clay minerals are few and known it can be useful in determining how a different factor influence the precipitation and dissolution of minerals because it was a closed system. The geothermal reservoir environment has a flow-through system, and thus this study recommends for the use of flow through autoclave as with such a system, the gas steam and the condensed water in the pipe flow out can be collected and measured for the changes in chemistry and evolution of such liquids. A further modification can be made to the system to determine the scaling effect and precipitation. The system also proved worthwhile working with although it can comfortably work under experiment for a day or two but getting it to 6 days or more running is a bit a matter of luck as the system can fail due to tear and wear. This research was not able to determine a solution to this, but regular monitoring of the set up can help reduce the liabilities to this effect.

Separation of the solution after the experiment proved a challenge and thus this study suggests using another method like the use of a centrifuge other than the one used here as this one may not be economical and consumes a lot of time although it minimizes the risk of sample contamination. The duration of the experiment was representative of a typical geothermal system as energy production occurs each day and the exchange of fluids in and out of the reservoir. As a recommendation, this study proposes an investigation of the behavior of K kaolinite and montmorillonite as a function of time under the same simulated hydrothermal conditions.

Valuable resources and software of interest to further on the topic can be found in the following articles. For example, the use of chemical activity plotting for mineral-solution equilibria ([Freeze, R.A., Cherry, 1979](#)). Saturation indices that can be used to determine the precipitation trend of minerals present in hydrothermal solution. These indices can be calculated using a program package called PHREEQC ([Parkhurst & Appelo, 1999](#)).

LIST OF REFERENCES

- Amin, N.-U., Alam, S., & Gul, S. (2014). Assessment of pozzolanic activity of thermally activated clay and its impact on strength development in cement mortar. *RSC Advances*. Retrieved from <http://pubs.rsc.org/en/content/getauthorversionpdf/C4RA12237B>
- AbuAisha, M., Loret, B., & Eaton, D. (2016). Enhanced Geothermal Systems (EGS): Hydraulic fracturing in a thermo-poroelastic framework. *Journal of Petroleum Science and Engineering*, *146*, 1179–1191. <https://doi.org/10.1016/j.petrol.2016.07.027>
- Alberto, C., Reyes, R., & Williams, C. D. (2010). Hydrothermal transformation of kaolinite in the system K₂O -SiO₂ -Al₂O₃ -H₂O. *55-63. Medellín*, *163*, 12–7353. Retrieved from <http://www.scielo.org.co/pdf/dyna/v77n163/a06v77n163.pdf>
- Aliyu, M. D., & Chen, H.-P. (2017). Sensitivity analysis of deep geothermal reservoir: Effect of reservoir parameters on production temperature. *Energy*, *129*, 101–113. <https://doi.org/10.1016/j.energy.2017.04.091>
- Ármansson, H. (2016). The fluid geochemistry of Icelandic high temperature geothermal areas. *Applied Geochemistry*, *66*, 14–64. <https://doi.org/10.1016/j.apgeochem.2015.10.008>
- Baba, A., & Ármannsson, H. (2006). Environmental Impact of the Utilization of Geothermal Areas. *Energy Sources, Part B: Economics, Planning, and Policy*, *1*(3), 267–278. <https://doi.org/10.1080/15567240500397943>
- Bartier, D., Ledesert, B., Clauer, N., Meunier, A., Liewig, N., Morvan, G., & Addad, A. (2008). Hydrothermal alteration of the Soultz-sous-Forets granite (Hot Fractured Rock geothermal exchanger) into a tosudite and illite assemblage. *European Journal of Mineralogy*, *20*(1), 131–142. <https://doi.org/10.1127/0935-1221/2008/0020-1787>
- Baysal, R. T., & Gunduz, O. (2016). The Impacts of Geothermal Fluid Discharge on Surface Water Quality with Emphasis on Arsenic. *Water, Air, & Soil Pollution*, *227*(5), 165. <https://doi.org/10.1007/s11270-016-2866-3>
- Björke, J. K., Stefánsson, A., & Arnórsson, S. (2015). Surface water chemistry at Torfajökull, Iceland—Quantification of boiling, mixing, oxidation and water–rock interaction and reconstruction of reservoir fluid composition. *Geothermics*, *58*, 75–86. <https://doi.org/10.1016/j.geothermics.2015.09.007>
- Bogie, I., Kusumah, Y. I., & Wisnandary, M. C. (2008). Overview of the Wayang Windu geothermal field, West Java, Indonesia. *Geothermics*, *37*(3), 347–365. <https://doi.org/10.1016/j.geothermics.2008.03.004>
- Brehme, M., Deon, F., Haase, C., Wiegand, B., Kamah, Y., Sauter, M., & Regenspurg, S. (2016). Fault controlled geochemical properties in Lahendong geothermal reservoir Indonesia. *Grundwasser*, *21*(1), 29–41. <https://doi.org/10.1007/s00767-015-0313-9>
- Brehme, M., Moeck, I., Kamah, Y., Zimmermann, G., & Sauter, M. (2014). A hydrotectonic model of a geothermal reservoir - A study in Lahendong, Indonesia. *Geothermics*, *51*, 228–239. <https://doi.org/10.1016/j.geothermics.2014.01.010>
- Browne, P. (1984). Lectures on geothermal geology and petrology, 93 p.
- Bundschuh, J., Maity, J. P., Nath, B., Baba, A., Gunduz, O., Kulp, T. R., ... Chen, C.-Y. (2013). Naturally occurring arsenic in terrestrial geothermal systems of western Anatolia, Turkey: Potential role in contamination of freshwater resources. *Journal of Hazardous Materials*, *262*, 951–959. <https://doi.org/10.1016/j.jhazmat.2013.01.039>
- Canet, C., Hernández-Cruz, B., Jiménez-Franco, A., Pi, T., Peláez, B., Villanueva-Estrada, R. E., ... Salinas, S. (2015). Combining ammonium mapping and short-wave infrared (SWIR) reflectance spectroscopy to constrain a model of hydrothermal alteration for the Acoculco geothermal zone, Eastern Mexico. *Geothermics*, *53*, 154–165. <https://doi.org/10.1016/J.GEOTHERMICS.2014.05.012>
- Çelik, A., Topçu, G., Baba, A., Akdoğan, Y., Şentürk, U., & Demir, M. M. (2017). Experimental modeling of silicate-based geothermal deposits. *Geothermics*, *69*, 65–73. <https://doi.org/10.1016/j.geothermics.2017.04.007>
- Clark, C. E., Harto, C. B., Sullivan, J. L., & Wang, M. Q. (2010). Water Use in the Development and Operation of Geothermal Power Plants.
- Clark, R. N., King, T. V. V., Klejwa, M., Swayze, G. A., & Vergo, N. (1990). High spectral resolution reflectance spectroscopy of minerals. *Journal of Geophysical Research*, *95*(B8). Retrieved from <https://pubs.er.usgs.gov/publication/70016091>

- Corrado, S., Aldega, L., Celano, A. S., De Benedetti, A. A., & Giordano, G. (2014). Cap rock efficiency and fluid circulation of natural hydrothermal systems by means of XRD on clay minerals (Sutri, Northern Latium, Italy). *Geothermics*, *50*, 180–188.
<https://doi.org/10.1016/j.geothermics.2013.09.011>
- Crisostomo, J. N. R., Villaseñor, L. B., & Calibugan, A. A. (2015). Developing the Acid Reservoir at Tiwi Geothermal Field, Philippines. *World Geothermal Congress 2015, 2005*(April), 10.
- Crowley, J. K., & Vergo, N. (1988). Near-Infrared reflectance spectra of mixtures of Kaolin-group minerals: Use in clay mineral studies. *Clays and Clay Minerals*, *36*(4), 310–316. Retrieved from
[http://www.clays.org/journal/archive/volume 36/36-4-310.pdf](http://www.clays.org/journal/archive/volume%2036/36-4-310.pdf)
- Duke, E. F. (1994). Near infrared spectra of muscovite, Tschermak substitution, and metamorphic reaction progress: Implications for remote sensing. *Geology*, *22*(7), 621.
[https://doi.org/10.1130/0091-7613\(1994\)022<0621:NISOMT>2.3.CO;2](https://doi.org/10.1130/0091-7613(1994)022<0621:NISOMT>2.3.CO;2)
- Elders, W. A., Bird, D. K., Williams, A. E., & Schiffman, P. (1984). Hydrothermal flow regime and magmatic heat source of the Cerro Prieto geothermal system, Baja California, Mexico. *Geothermics*, *13*(1–2), 27–47. [https://doi.org/10.1016/0375-6505\(84\)90005-1](https://doi.org/10.1016/0375-6505(84)90005-1)
- Fang, Z.-J., Zhai, X.-S., Li, Z.-L., Pan, R.-J., & Mo, M. (2017). Pressure dependence of the electronic structure in kaolinite: A first-principles study. *Modern Physics Letters B*, *31*(175019410).
<https://doi.org/10.1142/S0217984917501949>
- Fatimah, I., Shaobin, W., & Dessy, W. (2011). ZnO/montmorillonite for photocatalytic and photochemical degradation of methylene blue. *Applied Clay Science*, *53*(4), 553–560.
<https://doi.org/10.1016/J.CLAY.2011.05.001>
- Fatimah, I., Wang, S., Narsito, & Wijaya, K. (2010). Composites of TiO₂-aluminum pillared montmorillonite: Synthesis, characterization and photocatalytic degradation of methylene blue. *Applied Clay Science*, *50*(4), 588–593. <https://doi.org/10.1016/J.CLAY.2010.08.016>
- Freeze, R.A., Cherry, J. A. (1979). *Groundwater*.
- Frick, S., Regenspurg, S., Kranz, S., Milsch, H., Saadat, A., Francke, H., ... Huenges, E. (2011). Geochemical and Process Engineering Challenges for Geothermal Power Generation. *Chemie Ingenieur Technik*, *83*(12), 2093–2104. <https://doi.org/10.1002/cite.201100131>
- García, L. A. G. (2013). Crystallinity variations of smectite-illite and kaolin hydrothermal alteration minerals by using SWIR spectroscopy. A study of the Rodalquilar Au-deposit, SE Spain., *60*, 84.
- García, R., Vigil De La Villa, R., Vegas, I., Frías, M., & Sánchez De Rojas, M. I. (2007). The pozzolanic properties of paper sludge waste. <https://doi.org/10.1016/j.conbuildmat.2007.03.033>
- Gunduz, O., Gurleyuk, H., Cakir, A., Elci, A., Baba, A., & Simsek, C. (2013). Sample Collection into Sterile Vacuum Tubes to Preserve Arsenic Speciation in Natural Water Samples. *Journal of Environmental Engineering*, *139*(8), 1080–1088. [https://doi.org/10.1061/\(ASCE\)EE.1943-7870.0000717](https://doi.org/10.1061/(ASCE)EE.1943-7870.0000717)
- Gunduz, O., Mutlu, M., Elci, A., Simsek, C., & Baba, A. (2012). The influence of geothermal fluid discharge on surface water quality: case study Simav Plain (Kütahya). *Çevre, Bilim ve Teknoloji Dergisi*. Retrieved from [https://scholar.google.com/scholar_lookup?title=The influence of geothermal fluid discharge on surface water quality%3A case study Simav Plain %28Kütahya%29&author=O. Gunduz&author=M. Mutlu&author=A. Elci&author=C. Simsek&author=A. Baba&journal=Çevre%2C Bilim ve Teknoloji Dergisi&volume=3&issue=4&pages=231-246&publication_year=2012](https://scholar.google.com/scholar_lookup?title=The%20influence%20of%20geothermal%20fluid%20discharge%20on%20surface%20water%20quality%3A%20a%20case%20study%20of%20Simav%20Plain%20in%20Kütahya%20Province%20and%20its%20implications%20for%20the%20environment&author=Gunduz&author=M.%20Mutlu&author=A.%20Elci&author=C.%20Simsek&author=A.%20Baba&journal=Çevre%20Bilim%20ve%20Teknoloji%20Dergisi&volume=3&issue=4&pages=231-246&publication_year=2012)
- Gunnlaugsson, E., Ármannsson, H., Thorhallsson, S., & Steingrímsson, B. (2014). Problems in geothermal operation – Scaling and Corrosion. Retrieved from <http://www.os.is/gogn/unu-gtp-sc/UNU-GTP-SC-18-19.pdf>
- Haraden, J. (1992). The status of hot dry rock as an energy source. *Energy*, *17*(8), 777–786.
[https://doi.org/10.1016/0360-5442\(92\)90121-F](https://doi.org/10.1016/0360-5442(92)90121-F)
- Hebert, R. L., Ledesert, B., Bartier, D., Dezayes, C., Genter, A., & Grall, C. (2010). The Enhanced Geothermal System of Soultz-sous-Forêts: A study of the relationships between fracture zones and calcite content. *Journal of Volcanology and Geothermal Research*, *196*(1–2), 126–133.
<https://doi.org/10.1016/j.jvolgeores.2010.07.001>
- Hedenquist, J., Arribas, A., & Gonzalez-Urien, E. (2000). Exploration for Epithermal Gold Deposits. *Reviews in Economic Geology*. <https://doi.org/07410123>
- Hodder, A. P. W. (2010). Geothermal Waters: A Source of Energy and Metals, 1–10. Retrieved from <http://nzic.org.nz/ChemProcesses/water/13A.pdf>
- Izquierdo, G., Arellano, V. M., Aragón, A., Portugal, E., & Martínez, I. (2000). Fluid acidity and

- hydrothermal alteration at the Los Humeros geothermal reservoir Puebla, Mexico. Retrieved from <https://www.geothermal-energy.org/pdf/IGAstandard/WGC/2000/R0151.PDF>
- Jedli, H., Jbara, A., Hedfi, H., Bouzgarrou, S., & Slimi, K. (2017). A laboratory study of supercritical CO₂ adsorption on cap rocks in the geological storage conditions. *Applied Physics A*, 123(4), 254. <https://doi.org/10.1007/s00339-017-0862-0>
- Klosek-Wawrzyn, E., Malolepszy, J., & Murzyn, P. (2013). Sintering behavior of kaolin with calcite. *Procedia Engineering*, 57(May), 572–582. <https://doi.org/10.1016/j.proeng.2013.04.073>
- Komadel, P. (2016). Acid activated clays: Materials in continuous demand. <https://doi.org/10.1016/j.clay.2016.05.001>
- Kopačková, V., & Koucká, L. (2017). Integration of Absorption Feature Information from Visible to Longwave Infrared Spectral Ranges for Mineral Mapping. *Remote Sensing*, 9(10), 1006. <https://doi.org/10.3390/rs9101006>
- Kruse, F. A., & Hauff, P. L. (1991). Identification of Illite Polytype Zoning in Disseminated Gold Deposits Using Reflectance Spectroscopy and X-Ray Diffraction—Potential for Mapping With Imaging Spectrometers. *IEEE Transactions on Geoscience and Remote Sensing*, 29(1), 101–104. <https://doi.org/10.1109/36.103298>
- Kuè, M., Vernoux, J.-F., Kellner, T., Isenbeck-Schroè, M., & Schulz, H. D. (1998). Onsite experimental simulation of brine injection into a clastic reservoir as applied to geothermal exploitation in Germany. *Applied Geochemistry*, 13(4), 477–490. Retrieved from http://ac.els-cdn.com/S0883292797000814/1-s2.0-S0883292797000814-main.pdf?_tid=4d943eea-9bb1-11e7-bf0a-00000aacb35d&acdnat=1505657327_0c1cca0bb1a37aa38e926413df56a675
- Kumari, W. G. P., Ranjith, P. G., Perera, M. S. A., Shao, S., Chen, B. K., Lashin, A., ... Rathnaweera, T. D. (2017). Mechanical behaviour of Australian Strathbogie granite under in-situ stress and temperature conditions: An application to geothermal energy extraction. *Geothermics*, 65, 44–59. <https://doi.org/10.1016/j.geothermics.2016.07.002>
- Ledesert, B., Berger, G., Meunier, A., Genter, A., & Bouchet, A. (1999). Diagenetic-type reactions related to hydrothermal alteration in the Soultz-sous-Forets Granite, France. *European Journal of Mineralogy*, 11(4). Retrieved from <http://eurjmin.geoscienceworld.org/content/11/4/731>
- Ledesert, B., Dubois, J., Genter, A., & Meunier, A. (1993). Fractal analysis of fractures applied to Soultz-sous-Forets hot dry rock geothermal program. *Journal of Volcanology and Geothermal Research*, 57(1–2), 1–17. [https://doi.org/10.1016/0377-0273\(93\)90028-P](https://doi.org/10.1016/0377-0273(93)90028-P)
- Ledesert, B., Dubois, J., Velde, B., Meunier, A., Genter, A., & Badri, A. (1993). Geometrical and fractal analysis of a three-dimensional hydrothermal vein network in a fractured granite. *Journal of Volcanology and Geothermal Research*, 56(3), 267–280. [https://doi.org/10.1016/0377-0273\(93\)90020-R](https://doi.org/10.1016/0377-0273(93)90020-R)
- Ledesert, B., Hebert, R., Genter, A., Bartier, D., Clauer, N., & Grall, C. (2010). Fractures, hydrothermal alterations and permeability in the Soultz Enhanced Geothermal System. *Comptes Rendus Geoscience*, 342(7–8), 607–615. <https://doi.org/10.1016/j.crte.2009.09.011>
- Ledesert, B., Hebert, R. L., Grall, C., Genter, A., Dezayes, C., Bartier, D., & Gerard, A. (2009). Calcimetry as a useful tool for a better knowledge of flow pathways in the Soultz-sous-Forets Enhanced Geothermal System. *Journal of Volcanology and Geothermal Research*, 181(1–2), 106–114. <https://doi.org/10.1016/j.jvolgeores.2009.01.001>
- Mechri, M. L., Chihi, S., Mahdadi, N., & Beddiaf, S. (2017). Study of Heat Effect on the Composition of Dunes Sand of Ouargla (Algeria) Using XRD and FTIR. *Silicon*, 9(6), 933–941. <https://doi.org/10.1007/s12633-015-9368-6>
- Miao, S., Ph, D., Shen, Z., Wang, X., Luo, F., Ph, D., ... Ph, D. (2017). Stabilization of Highly Expansive Black Cotton Soils by Means of Geopolymerization. *Journal of Materials in Civil Engineering*, 29(10), 1–9. [https://doi.org/10.1061/\(ASCE\)MT.1943-5533.0002023](https://doi.org/10.1061/(ASCE)MT.1943-5533.0002023)
- Mortensen, J. J. (1978). Hot dry rock: a new geothermal energy source. *Energy*, 3(5), 639–644.
- Na, J., Xu, T., Jiang, Z., Bao, X., Yongdong, W., & Feng, B. (2016). A study on the interaction of mud acid with rock for chemical stimulation in an enhanced geothermal system. *Environmental Earth Sciences*, 75(12), 1025. <https://doi.org/10.1007/s12665-016-5827-7>
- Ngo, V. V., Lucas, Y., Clement, A., & Fritz, B. (2016). Modeling the impact of temperature on the saturation state and behavior of minerals in the Soultz-sous-Forets geothermal system. *Geothermics*, 64, 196–208. <https://doi.org/10.1016/j.geothermics.2016.06.001>
- Parkhurst, D. L., & Appelo, C. A. J. (1999). User's guide to PHREEQC (Version 2) : a computer program for speciation, batch-reaction, one-dimensional transport, and inverse geochemical calculations. *Water-Resources Investigations Report*. Retrieved from <https://pubs.er.usgs.gov/publication/wri994259>

- Patrier, P., Bruzac, S., Pays, R., Beaufort, D., Bouchot, V., Verati, C., & Gadalia, A. (2013). Occurrence of K-feldspar-bearing hydrothermal breccias in the Bouillante geothermal field (Basse Terre - Guadeloupe). *Bulletin de La Societe Geologique de France*, 184(1–2), 119–128. <https://doi.org/10.2113/gssgfbull.184.1-2.119>
- Pauwels, H., Fouillac, C., & Fouillac, A.-M. (1993). Chemistry and isotopes of deep geothermal saline fluids in the Upper Rhine Graben: Origin of compounds and water-rock interactions, 51, 2737–2749. Retrieved from http://ezproxy.utwente.nl:2819/001670379390387C/1-s2.0-001670379390387C-main.pdf?_tid=f2ff399a-4aec-11e7-ab3b-00000aab0f6c&acdnat=1496776900_6dfb9c5aed70d9427d7e636bd3558d85
- Post, J. L., & Noble, P. N. (1993). The Near-Infrared combination band frequencies of dioctahedral smectites, micas and illites. *Clays and Clay Minerals*, 41(6), 639–644. Retrieved from http://www.clays.org/journal/archive/volume_41/41-6-639.pdf
- Rani, N., Ravibabu Mandla, V., & Singh, T. (2017). Spatial distribution of altered minerals in the Gadag Schist Belt (GSB) of Karnataka, Southern India using hyperspectral remote sensing data. *Geocarto International*, 32(3), 225–237. <https://doi.org/10.1080/10106049.2015.1132484>
- Regenspurg, S., Geigenmüller, I., Milsch, H., & Kühn, M. (2017). Copper precipitation as consequence of steel corrosion in a flow-through experiment mimicking a geothermal production well. *Geothermal Energy*, 5. <https://doi.org/10.1186/s40517-017-0069-9>
- Rosenbauer, R. J., Koksalan, T., & Palandri, J. L. (2005). Experimental investigation of CO₂-brine-rock interactions at elevated temperature and pressure: Implications for CO₂ sequestration in deep-saline aquifers. *Fuel Processing Technology*, 86(14–15), 1581–1597. <https://doi.org/10.1016/j.fuproc.2005.01.011>
- S.A.Carroll, M. M. S. (2015). CarrollFY15LLNL_GTO_26Oct2015.
- Santos, S. S. G., Silva, H. R. M., De Souza, A. G., Alves, A. P. M., Da, E. C., Filho, S., & Fonseca, M. G. (2015). Acid-leached mixed vermiculites obtained by treatment with nitric acid. *Applied Clay Science*, 104, 286–294. <https://doi.org/10.1016/j.clay.2014.12.008>
- Schmidt, R. B., Bucher, K., Mundhenk, N., & Stober, I. (2017). Reactivity of Geothermal Reservoir Rocks under Temperature Conditions Found in the Upper Rhine Graben (Germany). *Procedia Earth and Planetary Science*, 17, 881–884. <https://doi.org/10.1016/j.proeps.2017.01.006>
- Shahwan, T., Erten, H. N., & Unugur, S. (2006). A characterization study of some aspects of the adsorption of aqueous Co²⁺ ions on a natural bentonite clay. *Journal of Colloid and Interface Science*, 300, 447–452. <https://doi.org/10.1016/j.jcis.2006.04.069>
- Steudel, A., Batenburg, L. F., Fischer, H. R., Weidler, P. G., & Emmerich, K. (2009). Alteration of swelling clay minerals by acid activation. Retrieved from <https://www.narcis.nl/publication/uquery/SurfaceANDareaANDclay/Language/EN/coll/publication/id/6/RecordID/oai:tudelft.nl:uuid:29458ad1-429f-4598-a4ab-e5764ba8a528>
- Tabak, A., Afsin, B., Aygun, S. F., & Icbudak, H. (2005). Phenanthroline Cu(II)-bentonite composite characterization. *Journal of Thermal Analysis and Calorimetry*, 81(2), 311–314. <https://doi.org/10.1007/s10973-005-0784-5>
- Thorhallsson, S. (2006). Common problems faced in geothermal generation and how to deal with them. Retrieved from <http://www.os.is/gogn/unu-gtp-sc/UNU-GTP-SC-02-25.pdf>
- van Ruitenbeek, F. J. A., Cudahy, T., Hale, M., & van der Meer, F. D. (2005). Tracing fluid pathways in fossil hydrothermal systems with near-infrared spectroscopy. *Geology*, 33(7), 597. <https://doi.org/10.1130/G21375.1>
- Wang, P., Chen, X., Shen, L., Wu, K., Huang, M., & Xiao, Q. (2016). Geochemical features of the geothermal fluids from the Mapamyum non-volcanic geothermal system (Western Tibet, China). <https://doi.org/10.1016/j.jvolgeores.2016.04.002>
- Wang, S., Chuan Lu, B., Dawa Nan, B., Xiancai Hu, B., & Jingli Shao, B. (2017). Geothermal resources in Tibet of China: current status and prospective development. *Environmental Earth Sciences*, 76. <https://doi.org/10.1007/s12665-017-6464-5>
- Zhao, H., Deng, Y., Harsh, J. B., Flury, M., & Boyle, J. S. (2004). Alteration of Kaolinite to Cancrinite and Sodalite by Simulated Hanford Tank Waste and its Impact on Cesium Retention. *Clays and Clay Minerals*, 52(1), 1–13. <https://doi.org/10.1346/CCMN.2004.0520101>
- Zhou, C., Remoroza, A. I., Shah, K., Doroodchi, E., & Moghtaderi, B. (2016). Experimental study of static and dynamic interactions between supercritical CO₂/water and Australian granites. *Geothermics*, 64, 246–261. <https://doi.org/10.1016/j.geothermics.2016.05.007>

7. APPENDICES

7.1.1. Appendix 1

Preparation of concentrations.

Ultrapure water was acquired from the ITC Geoscience lab. The other solutions were prepared at the University of Twente High Pressure Lab. 1M sodium chloride was prepared using 100g of ultrapure water and 5.8g of pure sodium chloride crystals. 1M potassium hydroxide was prepared using 100g of ultrapure water and 5.6g of potassium hydroxide pellets. This was done to prevent different concentrations used in the experiments i.e. have a homogenous concentration for all the experiments.

7.1.2. Appendix 2

Table 11. Showing the extracted reflectance values for Kaolinite used to calculate the crystallinity index (KX) using the equation stated in the methodology. The three spectra were zoomed, and the values manually extracted in ENVI and recorded in the table below.

sample	2166 D	2177 D	2184 D	2190 D	2166D/2177 D	2184D/2190 D	2184D/2190 D - 2166D/2177 D	KX
Kao.OD	0.673	0.680	0.673	0.654	0.990	1.029	0.039	0.990
Kao.W.R	0.664	0.672	0.666	0.648	0.988	1.028	0.040	0.988
Kao.N.R.	0.642	0.649	0.642	0.623	0.989	1.030	0.041	0.989
Kao.K.R.	0.754	0.754	0.744	0.726	1.000	1.025	0.025	0.975

7.1.3. Appendix 3

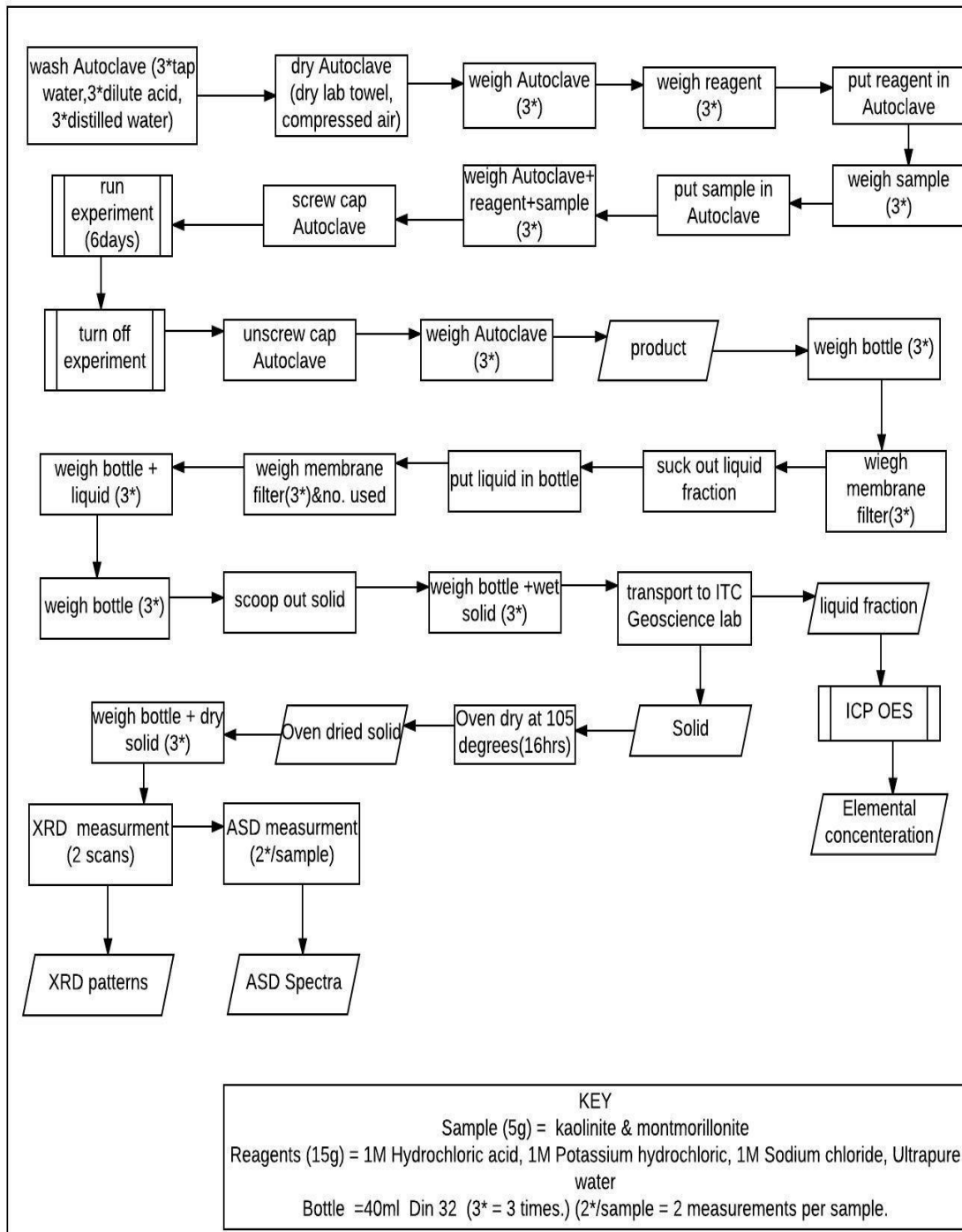
Table 12. Showing extracted reflectance values for Montmorillonite used to calculate its crystallinity index using the equation stated in the methodology. The text in bold are the positions at which the reflectance values were extracted from. The reflectance values were manually extracted from ENVI while the asymmetry was extracted using IDL DISPEC plugin software of the same ENVI.

Sample	1400AS	2200D (2209)	1900D (1904)	2200D/1900D	1 + 1400AS	Montmorillonite crystallinity
Mont.OD	0.199	0.578	0.563	1.027	1.199	1.231
Mont.W.R.	0.150	0.573	0.565	1.018	1.150	1.171
Mont.N.R.	0.116	0.603	0.619	0.974	1.116	1.146
Mont.K.R.	0.060	0.740	0.775	0.955	1.060	1.055

7.1.4. Appendix 4

Flowchart illustrating the steps taken in the process used to conduct the experiment. The solid sample represents all the solids used in analysis even the unreacted samples as all the analysis and modifications done was same to all the samples and done at the ITC Geoscience lab while the experiment was

conducted at the University of Twente, High Pressure Lab. The weight of the autoclave after sample extraction was also measured before cleaning of the autoclave was done.



7.1.5. Appendix 5

The standard operating procedure used in the entire experiment.

Standard operating procedure

1. Sample preparation

1.1. Clean autoclave 3 times with tap water, 3 times dilute acid and 3 times ultrapure water

- 1.2. Dry it with air and a dry lab tissue.
- 1.3. Make sure the vessel and screw thread are clean
- 1.4. Apply grease on the bottom threads and close till it clicks
- 1.5. Measure autoclave and record the weight
- 1.6. Add 15 ml reagent to the autoclave
- 1.7. Measure and record the weight
- 1.8. Add either 5.0-gram Kaolin or Montmorillonite to the autoclave
- 1.9. Measure and record the weight
- 1.10. Use oil on screw thread and lid
- 1.11. Close vessel using torque wrench
2. Set-up preparation
 - 2.1. Turn on ventilation
 - 2.2. Switch on power
 - 2.3. Switch on set-up
 - 2.4. Set oven temperature at 260 °C
 - 2.5. Open LP N₂, HP N₂, Air and fluidization gas
 - 2.6. Switch on pre-heater and set temperature at 300 °C
 - 2.7. Raise set-up if needed
 - 2.8. Attach vessel to set-up
 - 2.9. Connect HP N₂ to pressure valve
 - 2.10. Connect gas line from pressure valve to vessel
 - 2.11. Connect thermocouple to vessel
3. Control procedure
 - 3.1. Apply a pressure of 200 bar to vessel
 - 3.2. Flush the system up to 3 times
 - 3.3. Check for leakage and pressure stability
 - 3.4. Release pressure
4. Main procedure
 - 4.1. Apply a pressure of 96 bar to the autoclave
 - 4.2. Disconnect HP N₂ from pressure valve
 - 4.3. Make sure all cables can move freely
 - 4.4. Exit bunker

- 4.5. Lower set-up into oven
- 4.6. Close HP N₂
- 4.7. Monitor for 6 days
5. Shutdown procedure
 - 5.1. Raise set-up, move set-up to bath and lower set-up into bath
 - 5.2. Check if the vessel has cooled to room temperature and reached a pressure of 96 bars
 - 5.3. Raise set-up
 - 5.4. Enter bunker
 - 5.5. Release pressure from vessel slowly
 - 5.6. Disconnect thermocouple from vessel
 - 5.7. Disconnect gas line from vessel
 - 5.8. Remove vessel from set-up
6. Sample extraction
 - 6.1. Open vessel using torque wrench
 - 6.2. Weigh autoclave
 - 6.3. Weigh membrane filter
 - 6.4. Connect the membrane filter to syringe
 - 6.5. Then connect the needle
 - 6.6. Suck out the liquid fraction using a syringe with a membrane filter
 - 6.7. Measure mass of the 40ml bottle to hold the liquid
 - 6.8. Inject the liquid from the syringe into the vessel
 - 6.9. Weigh membrane filter and the number used.
 - 6.10. Measure and record the weight of the 40ml bottle + liquid
 - 6.11. Scoop out the solid from autoclave
 - 6.12. Measure the weight of the empty autoclave
 - 6.13. Measure and record mass of the 40ml bottle
 - 6.14. Put the scooped out solid into the 40ml bottle
 - 6.15. Measure and record weight of new contents in 40ml bottle
 - 6.16. Prepare samples for transport (to the ITC Geoscience lab)
 - 6.16.1. Oven dry the sample in the petri dish overnight at 105°C
 - 6.16.2. Remove sample and measure with XRD
 - 6.16.3. Measure sample with ASD

- 6.16.4. Measure contents in the liquid fraction using the ICP-OES
- 6.17. Clean vessel and screw thread and start again procedure with brine, KOH and HCL in that order.
(one reagent per week per sample)
7. Complete shutdown (after the follow-up experiments are done)
 - 7.1. Close LP N₂ and Air
 - 7.2. Switch off power
 - 7.3. Turn off ventilation
8. Emergency shut down in case of calamity

7.1.6. Appendix 6

Table 13. Showing the concentration values for each element present in the original and residues of the Kaolinite sample from each experiment. Where the first values alongside each sample represent the concentration in micro gram per gram for each element.

	Mg	Ca	Fe	Al	Si
Kao.OD	379.41	226.62	3236.11	281915.55	306513.42
%weight	0.06406019	0.03826288	0.54638998	47.5990716	51.7522153
molecular proportions	0.00158919	0.00068229	0.00337904	0.46684064	0.86124505
atom/oxygen proportions	0.00158919	0.00068229	0.01013711	1.40052192	1.72249011
	0.00456165	0.00195847	0.02909783	4.02009773	4.94428432
ions	0.00456165	0.00195847	0.01939856	2.68006515	2.47214216
			0.91122215	1.768843	
Kao.W.R	525.94	175.98	3980.93	242920.72	271544.84
%weight	0.10130822	0.03389782	0.76681926	46.7921533	52.3058214
molecular proportions	0.00251323	0.00060445	0.00474223	0.45892657	0.870458
atom/oxygen proportions	0.00251323	0.00060445	0.0142267	1.37677972	1.74091601
	0.00721492	0.00173525	0.04084169	3.95242709	4.99778105
ions	0.00721492	0.00173525	0.02722779	2.63495139	2.49889053
			0.89588347	1.73906792	
Kao.N.R	667.15	160.31	3457.72	222581.96	245557.24
%weight	0.14121837	0.03393347	0.73190973	47.1148335	51.9781049
molecular proportions	0.00350331	0.00060509	0.00452634	0.46209134	0.86500424
atom/oxygen proportions	0.00350331	0.00060509	0.01357903	1.38627403	1.73000849
	0.01006065	0.00173767	0.03899567	3.9810421	4.9681639
ions	0.01006065	0.00173767	0.02599712	2.65402807	2.48408195
			0.90236954	1.75165852	
Kao.K.R	640.42	197.32	3026.82	209757.48	229879.33
%weight	0.14440091	0.04449141	0.68248267	47.2957908	51.8328342

molecular proportions	0.00358226	0.00079336	0.00422067	0.46386613	0.86258669
atom/oxygen proportions	0.00358226	0.00079336	0.01266202	1.39159839	1.72517338
	0.01028791	0.00227844	0.0363641	3.9965371	4.95453246
ions	0.01028791	0.00227844	0.02424273	2.66435806	2.47726623
			0.90588174	1.75847632	

7.1.7. Appendix 7

Table 14. Showing the concentration values for each element present in the original and residues of the Montmorillonite samples from each experiment. Where the first values alongside each sample represent the concentration in micro gram per gram for each element.

	Mg	K	Ca	Fe	Al
Mont.OD	6968.76		1029.81	11923.31	80809.18
%weight	1.337700143		0.19767892	2.28875919	15.5118632
molecular proportions	0.033185317		0.00352495	0.01415435	0.15213675
atom/oxygen proportions	0.033185317		0.00352495	0.04246306	0.45641025
	0.133963163		0.01422957	0.17141576	1.84244618
ions	0.133963163		0.01422957	0.11427717	1.22829745
				0.41762113	0.81067632
Mont.W.R	6127.39		844.56	11548.58	79175.86
%weight	1.264013004		0.17422342	2.38234473	16.333107
molecular proportions	0.031357306		0.00310669	0.01473312	0.16019132
atom/oxygen proportions	0.031357306		0.00310669	0.04419935	0.48057396
	0.126723965		0.01255505	0.17862237	1.94213871
ions	0.126723965		0.01255505	0.11908158	1.29475914
				0.44021811	0.85454103
Mont.N.R	5371.79		431.23	11979.98	69958.97
%weight	1.2000661		0.09633744	2.67634585	15.6289409
molecular proportions	0.029770928		0.00171786	0.0165513	0.15328502
atom/oxygen proportions	0.029770928		0.00171786	0.04965391	0.45985507
	0.120307983		0.00694207	0.20065757	1.85833091
ions	0.120307983		0.00694207	0.13377171	1.23888728
				0.42122167	0.8176656
Mont.K.R	5855.04	2102.35	1016.65	10965.72	75678.26
%weight	1.24317292	0.446382021	0.21586048	2.32829941	16.0684066

molecular proportions	0.030840311	0.004738663	0.00384915	0.01439888	0.1575952
atom/oxygen proportions	0.030840311	0.004738663	0.00384915	0.04319665	0.4727856
	0.134588734	0.020679773	0.0167979	0.18851245	2.06326118
ions	0.134588734	0.041359545	0.0167979	0.12567496	1.37550745
				0.46767253	0.90783492

